Innovative Fresh Water Production Process for Fossil Fuel Plants

Annual Report

Reporting Period: 9/30/03-9/30/04

Principal Investigators: James F. Klausner and Renwei Mei
Graduate Student: Yi Li,
Undergraduate Student: Jessica Knight

September 2004

University of Florida
Department of Mechanical and Aerospace Engineering
Gainesville, Florida 32611

Disclaimer*

Abstract
An innovative Diffusion Driven Desalination (DDD) process was recently described where evaporation of mineralized water is driven by diffusion within a packed bed. The energy source to drive the process is derived from low pressure condensing steam within the main condenser of a steam power generating plant. Since waste heat is used to drive the process, the main cost of fresh water production is attributed to the energy cost of pumping air and water through the packed bed. This report describes the annual progress made in the development and analysis of a Diffusion Driven Desalination (DDD) system. A combined thermodynamic and dynamic analysis demonstrates that the DDD process can yield a fresh water production of 1.03 million gallon/day by utilizing waste heat from a 100 MW steam power plant based on a condensing steam pressure of only 3" Hg. Throughout the past year, the main focus of the desalination process has been on the diffusion tower and direct contact condenser. Detailed heat and mass transfer analyses required to size and analyze these heat and mass transfer devices are described. An experimental DDD facility has been fabricated, and temperature and humidity data have been collected over a range of flow and thermal conditions. The analyses agree quite well with the current data and the information available in the literature. Direct contact condensers with and without packing have been investigated. It has been experimentally observed that the fresh water production rate is significantly enhanced when packing is added to the direct contact condensers.

Table of Contents

1. Introduction

A desalination technology that has drawn interest over the past two decades is referred to as Humidification Dehumidification (HDH). This process operates on the principle of mass diffusion and utilizes dry air to evaporate saline water, thus humidifying the air. Fresh water is produced by condensing out the water vapor, which results in dehumidification of the air. A significant advantage of this type of technology is that it provides a means for low pressure, low temperature desalination that can operate off of waste heat and is potentially very cost competitive. Bourouni et al. [1], Al-Hallaj et al. [2], and Assouad et al. [3] respectively reported on the operation of HDH units in Tunisia, Jordan, and Egypt. Muller-Holst [4] fabricated an experimental Multi Effect Humidification (MEH) facility driven by solar energy and considered its performance over a wide range of operating conditions. Since the process is driven by solar energy, the fresh water production varied with seasonal changes. The average fresh water production was about 6,000 liters per month with a maximum of 10,500 liters in May and a minimum of 1,700 liters in January. A computer simulation of the operational performance of the process was developed, and the predicted behavior agreed with the actual behavior. An excellent comprehensive review of the HDH process is provided by Al-Hallaj and Selman [5]. It was concluded that although the HDH process operates off of low grade energy, it is currently not cost competitive with reverse osmosis (RO) and multistage flash evaporation (MSF). There are three primary reasons for the higher costs associated with the HDH process:

1) The HDH process is typically applied to low production rates and economies of scale that cannot be realized in construction.
2) Typically natural draft is relied upon, which results in low heat and mass transfer coefficients and a larger surface area humidifier.
3) Film condensation over tubes is typically used, which is extremely inefficient when non-condensable gases are present. Thus a much larger condenser area is required for a given production rate, and the condenser accounts for the majority of the capital cost.

Therefore, an economically feasible diffusion driven distillation process must overcome these shortcomings. Klausner et al. [6] have reported on a diffusion driven desalination (DDD) process that overcomes these shortcomings, resulting in an economically viable desalination process applied on a large scale (>1 million gallons per day).

Another type of desalination technology that makes use of water evaporating into an air stream is the Carrier-Gas Process (CGP) reported by Larson et al. [7]. This process has been further refined by Beckman [8] [9] with financial support from the Bureau of Reclamation. The CGP is designed to operate with a feed water temperature range of 55-88°C. Beckman demonstrates (based on 88°C feed water) that the CGP can produce fresh water with an operating cost of $3.35 per 1000 gallons using natural gas for heating and $1.52 when waste heat is used as the thermal source. The capital cost is quite low, approximately $1,397 for a 1000 gallon per day facility. Based on this outcome, the CGP should readily find commercial success.

1.1 Description of DDD Process

A simplified schematic diagram of the DDD process and system, designed to be operated off of the waste heat discharged from electricity generating power plants, is shown in Fig. 1. The system described here, which is currently under development, is designed for large scale production. A main feed pump(a) draws water from a large body of seawater. The suction for the pump draws water from near the surface in order to take advantage of the fact that large bodies of water absorb solar radiation, and due to thermal stratification, the warmer water is in the vicinity of the surface, while cooler water resides at depths further below the surface. The surface water is pumped through the main feed water heater (b) where the amount of heat required depends on the main feed water mass flow rate and desired production rate. The required output temperature of the heater is relatively low and therefore the required heat input can be provided by a variety of sources, depending on the available resources. It is envisioned that heat can be provided from low pressure condensing steam in a power plant, exhaust from a combustion engine, waste heat from an oil refinery, or other waste heat sources. After the feed water is heated in the main heater, it is sprayed into the top of the diffusion tower (c). The diffusion tower is one of the most important pieces of equipment in the process, and the degree to which an operational DDD process follows theoretically predicted trends depends on an appropriately designed diffusion tower. On the bottom of the diffusion tower, low humidity air is pumped in using a forced draft blower (d). The water falls countercurrent to the airflow through the diffusion tower by means of gravity. The diffusion tower is packed with very high surface area packing material. As water flows through the diffusion tower, a thin film of water forms over the packing material and makes contact with the air flowing upward through the tower. As dictated by Fick's law and the conservation of mass, momentum, and energy, liquid water will evaporate and diffuse into the air, while air will diffuse into the water, due to concentration gradients. The diffusion tower should be designed such that the air/vapor mixture leaving the diffusion tower be fully saturated. The purpose of heating the water prior to entering the diffusion tower is that the rate of diffusion and the exit humidity ratio will increase with increasing temperature, thus yielding greater production. The water not evaporated in the diffusion tower, will be collected at the bottom and removed with a brine pump (e). The brine will be discharged.

Another very important component of the DDD process is the condenser. The air entering the diffusion tower will be dried in the direct contact condenser (g). The saturated air/vapor mixture leaving the diffusion tower is drawn into the direct contact condenser with a forced draft blower (f), where the water vapor is condensed into fresh liquid water that is collected in the sump of the condenser. The difficulty that arises is that film condensation heat transfer is tremendously degraded in the presence of non-condensable gas. The same difficulty was faced in the design and development of condensers for OTEC (Ocean Thermal Energy Conversion) applications. In order to overcome this problem Bharathan et al. [10] describe the use of direct-contact heat exchangers. In their excellent report they have developed models for simulating the heat transfer in a direct contact condenser and have validated the models with careful experimentation. For the current desalination application, the warm fresh water discharging from the direct contact heat exchanger will be chilled in a conventional shell-and-tube heat exchanger (h) using saline cooling water. The cooling water is drawn from

a deeper depth to take advantage of the thermal stratification in large bodies of water. A portion of the chilled fresh water will be directed back to the direct contact heat exchanger to condense the water vapor from the air/vapor mixture discharging from the diffusion tower. The rest of the fresh water is make-up water. The direct contact condenser approach is best suited for the DDD process.

Figure 1 Flow Diagram of Diffusion Driven Desalination Process

1.2 Advantages of the DDD Process Compared with HDH and MEH

1) The DDD process utilizes thermal stratification in the seawater to provide improved performance. In fact, the DDD process can produce fresh water without any additional heating by utilizing the seawater thermal stratification.

2) The thermal energy required for the DDD process may be entirely driven by waste heat therefore eliminating the need for additional heating sources. This helps keep the DDD plant compact, which translates to reduced cost. The DDD process recommends using the heat source that is best suited for the region requiring fresh water production. The DDD process is very well suited to be integrated with steam power plants, specifically in using the waste heat generated from these plants. The current proposed project will focus on using solar heating, wind energy, and geothermal energy resources to drive the desalination process.

3) In the DDD process the evaporation occurs in a forced draft packed bed diffusion tower as opposed to a natural draft humidifier. The diffusion tower is packed with low pressure-drop, high surface area packing material, that provides significantly

greater surface area. This is very important because the rate of water evaporation is directly proportional to the liquid/vapor surface area available. In addition, the forced draft provides for high heat and mass transfer coefficients. Thus, a diffusion tower is capable of high production rates in a very compact and low capital cost unit. The price paid in using forced draft is the pumping power required to pump the fluids through the system, but the projected cost is low, thus providing the potential for an economically competitive desalination technology.

4) The DDD process uses a direct contact condenser to extract fresh water from the air/water vapor mixture. This type of condenser is significantly more efficient than the conventional tube condenser, as is used with the HDH process. Thus, the condenser will be considerably more compact for a given design production rate, resulting in reduction of cost.

5) The diffusion tower and direct contact condenser can accommodate very large flow rates, and thus economies of scale can be taken advantage of to produce large production rates.

6) No specialized components are required to manufacture a DDD plant. All of the components required to fabricate a DDD plant are manufactured in bulk and are readily available from different suppliers. This facet of production also translates to reduced cost.

1.3 Disadvantage of the DDD Process

The fraction of feed water converted to fresh water using the DDD process is largely dependent on the difference in high and low temperatures in the system. When driving the process using low grade waste heat, this temperature difference will be moderate. Thus the fraction of feed water converted to fresh water will be low. A large amount of water and air must be pumped through the facility to accomplish a sizable fresh water production rate. This disadvantage is an inherent characteristic of the DDD process. However, as long as the production cost of fresh water using the DDD process is cost competitive, it is a tolerable characteristic.

2. Experimental Facility

In the 2003 annual report by Klausner et al [11], a diffusion driven desalination facility was described and its performance based on thermodynamic and dynamic transport considerations was discussed. In addition, a design and optimization procedure for the diffusion tower performance was developed. Through continuing research, there are several main research objectives for the DDD project this year. One major research objective is to develop an experiment to validate the analytical model of the DDD process. Another major objective is to construct a direct contact condenser experimental facility to examine the actual fresh water production efficiency of the entire DDD process. Currently, these two objectives have been successfully achieved and are described in detail within the report. The conclusions drawn from the analytical investigation of the diffusion tower are validated by the experiments. The original analytical model was calibrated using the experimental data. It should also be noted that the performance of the overall direct contact condenser has a strong influence on the overall performance of the DDD process.

The initial focus of the experimental investigation was on the diffusion tower. After the performance of the diffusion tower had been thoroughly investigated, a direct contact condenser was added. The objectives of the experimental investigation are as follows:

a) Fabricate a laboratory scale diffusion driven desalination facility, including the diffusion tower and the new direct contact condenser.
b) Provide sufficient instrumentation such that detailed heat and mass transfer measurements may be made as well as measurements of fresh water production and energy consumption.
c) Conduct an array of experiments over the range of parameter space considered in the analysis, and make extensive measurements of heat and mass transfer coefficients, pressure drop, and evaporation rate.
d) Compare the experimental results with the analytical results.
e) Develop a dimensionless correlation for the heat transfer coefficient for air and water flow through packed beds. Make adjustments to the analytical model as required.
f) Investigate the performance of the direct contact condenser, and investigate the real fresh water production efficiency of the DDD experimental facility.
g) Modify the structure of the direct contact condenser to make it more efficient.

Fig. 2 shows a pictorial view of the laboratory-scale DDD system. Fig. 3 shows a schematic diagram of the experimental facility. The main feed water, which simulates the seawater, is drawn from one municipal water line. The feed water initially passes through a vane type flow meter and then enters a preheater which is capable of raising the feed water temperature to 50° C. The feed water then flows through the main heater, which can raise the temperature to saturated conditions. The feed water temperature is controlled with a PID feedback temperature controller where the water temperature is measured at the outlet of the main heater. The feed water is then sent to the top of the diffusion tower, where it is sprayed over the top of the packing material. The water sprayed on top of the packing material gravitates downward and that which is not evaporated is collected at the bottom of the diffusion tower in a sump and discharged through a drain. The temperature of the discharge water is measured with a thermocouple. Strain gauge type pressure transducers are mounted at the bottom and top of the diffusion tower to measure the static pressure. A magnetic reluctance differential pressure transducer is used to measure the pressure drop across the length of the packing material.

Dry air is drawn into a centrifugal blower equipped with a 1.11 kW (1.5 horsepower) motor. The discharge air from the blower flows through a 10.2 cm duct in which a thermal mass flow meter is inserted. The air flow rate is controlled by varying the speed of the blower. A three-phase autotransformer is used to control the voltage to the motor and therefore regulate the speed. Downstream of the thermal mass flow meter the temperature and inlet relative humidity of the air are measured with a thermocouple and a resistance type humidity gauge. The air is forced through the packing material in the diffusion tower and discharges through a duct at the top of the diffusion tower. At the top of the tower, the temperature and humidity of the discharge air are measured in the same manner as at the inlet.
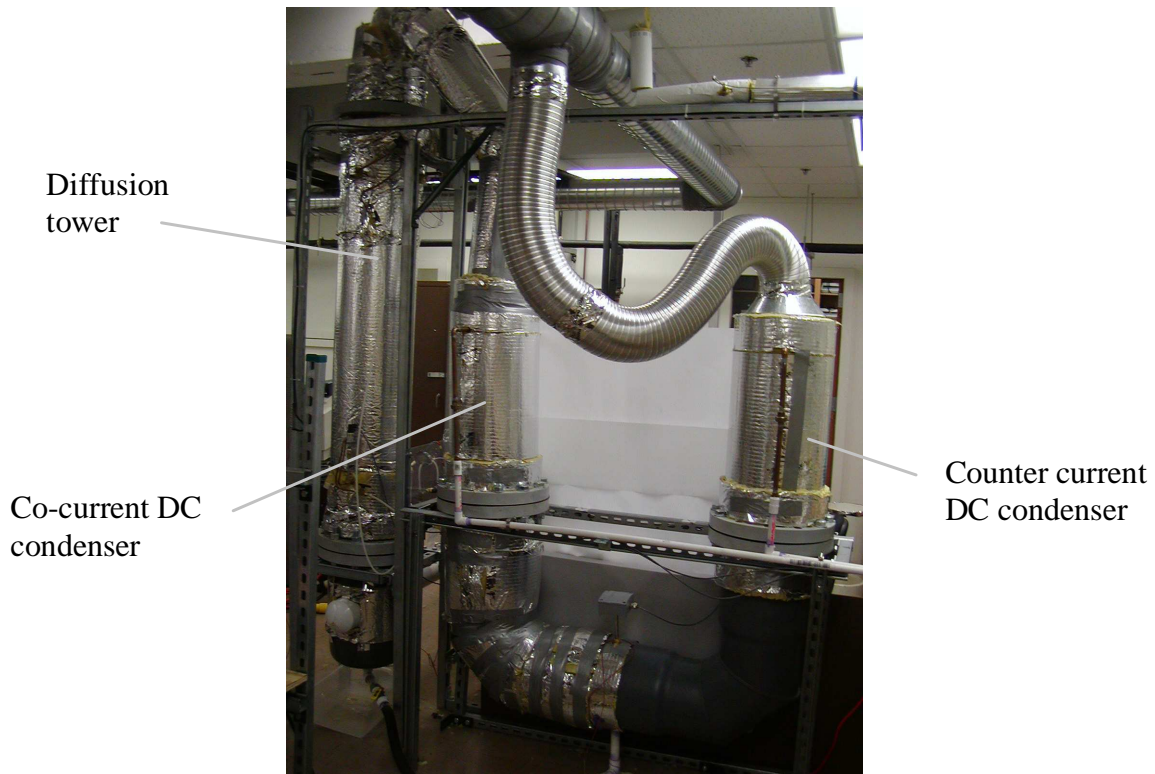
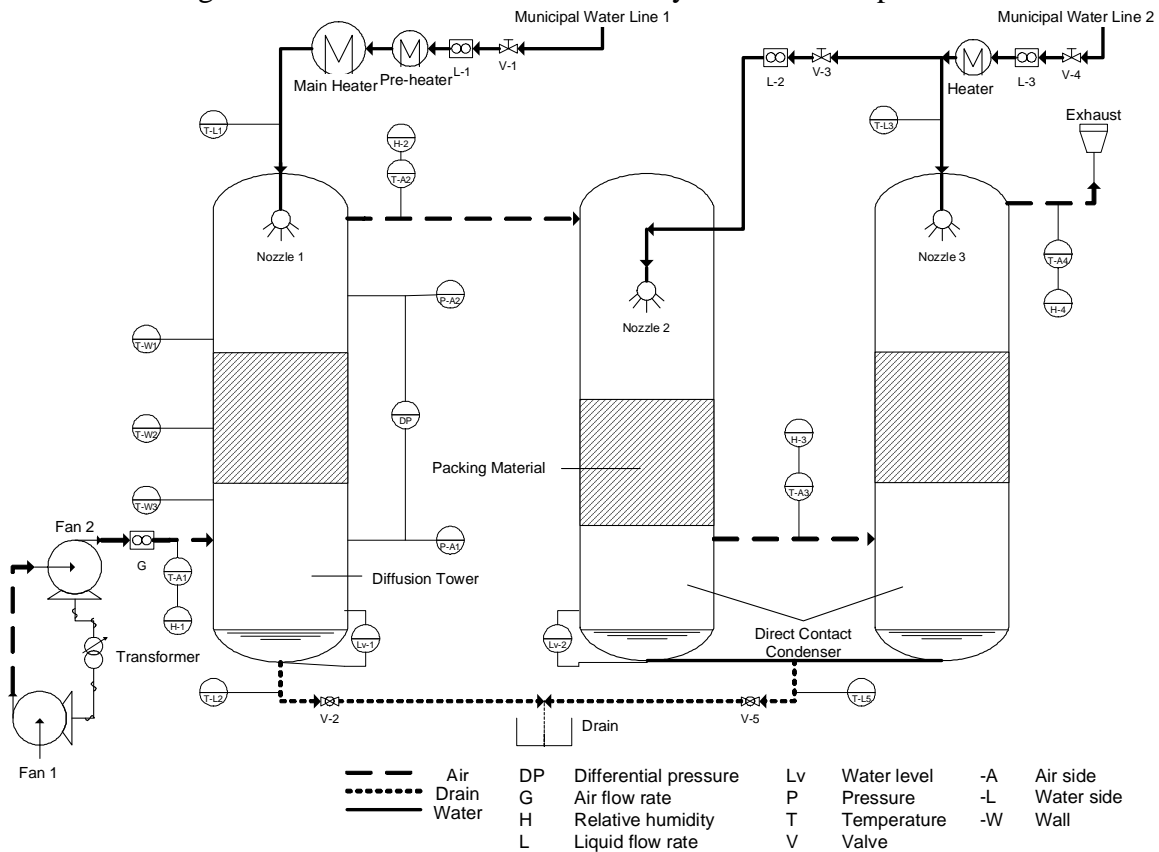Figure 2 Pictorial view of the laboratory-scale DDD experiment

Figure 3 Schematic diagram of DDD facility

The condenser is designed to consist of two stages in a twin tower structure. The main feed water, which simulates the cold fresh water, is drawn from another municipal water line. The feed fresh water is separated into two waterlines and passes through two different turbine flow meters. After the fresh water temperature is measured at the inlet of the condenser tower, it is sprayed from the top of each tower.

The air drawn by the centrifugal blower flows out of the top of the diffusion tower with an elevated temperature and absolute humidity. It then flows into the first stage of the direct contact condenser, which is also called the concurrent flow stage. Here, the cold fresh water and wet air will have heat and mass exchange as they both flow to the bottom of this tower. The twin towers are connected by two PVC elbows where the temperature and relative humidity of air are measured by a thermocouple and a resistance type humidity gauge. The air is then drawn into the bottom of the second stage of the condenser. Because the fresh water is sprayed from the top and the wet air comes from the bottom, this stage of the condenser is denoted as the countercurrent flow stage. The air will continue being cooled down and dehumidified by the cold fresh water until it is discharged at the top of the second stage. At this outlet, the temperature and humidity of the discharge air are measured in the same manner as at the inlet.

The water sprayed on top of the condenser gravitates toward the bottom. The portion of the water condensate from the vapor is collected together with the initial inlet cold fresh water at the bottom of the twin towers and discharged through a drain. The temperature of the discharge water is measured with a thermocouple.

There are two optional components of the condenser. One is a traditional fin tube surface condenser and the other is the packing material. Whether or not they are required depends on the fresh water production efficiency yielded by the direct contact condenser.

2.1 Description of Individual Components

Diffusion Tower

       A rendered view of the diffusion tower is shown in Fig. 4 and a CAD design is shown in Fig. 5. The diffusion tower consists of three main components: a top chamber containing the air plenum and spray distributor, the main body containing the packing material, and the bottom chamber containing the air distributor and water drain. The top and bottom chambers are constructed from 25.4 cm (10" nominal) ID PVC pipe and the main body is constructed from 24.1 cm ID acrylic tubing with wall thickness of 0.64 cm. The three sections are connected via PVC bolted flanges. The transparent main body accommodates up to 1 m of packing material along the length.

Figure 4 Rendered view of the experimental diffusion tower

No.	Device
17	PVC connection
16	Humidity test port
15	Air exhaust port
14	Top hatch
13	Water inlet port
12	Top flanges
11	Pressure test port
10	Acrylic Wall
09	Packing material
08	Pressure test port
07	Bottom flanges
06	Air inlet pipe hatch
05	Water level test port
04	Water level test port
03	Bottom hatch
02	Drain port
01	Air inlet pipe
No.	Device
Diffusion tower design	
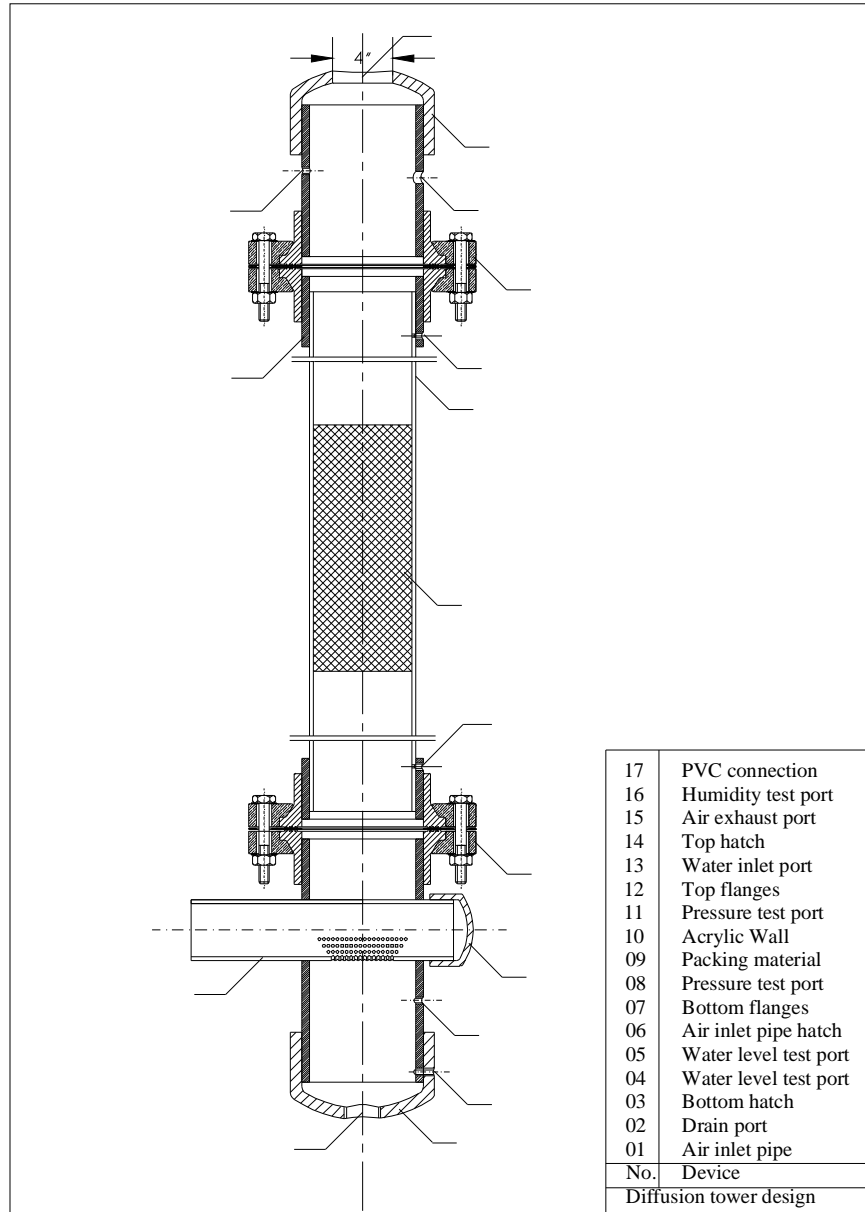
Figure 5 Schematic diagram of experimental diffusion tower

Direct contact condenser

A CAD design of the direct contact condenser is shown in Fig. 6. The condenser includes two towers. Each tower consists of two main components: a top chamber containing the air plenum and spray distributor, and a bottom chamber containing the packing material and water drain. The top chamber is constructed from 25.4 cm (10" nominal) ID acrylic tubing and the bottom chamber is constructed from 25.1 cm ID PVC pipe. The two sections are connected via PVC bolted flanges. The transparent body accommod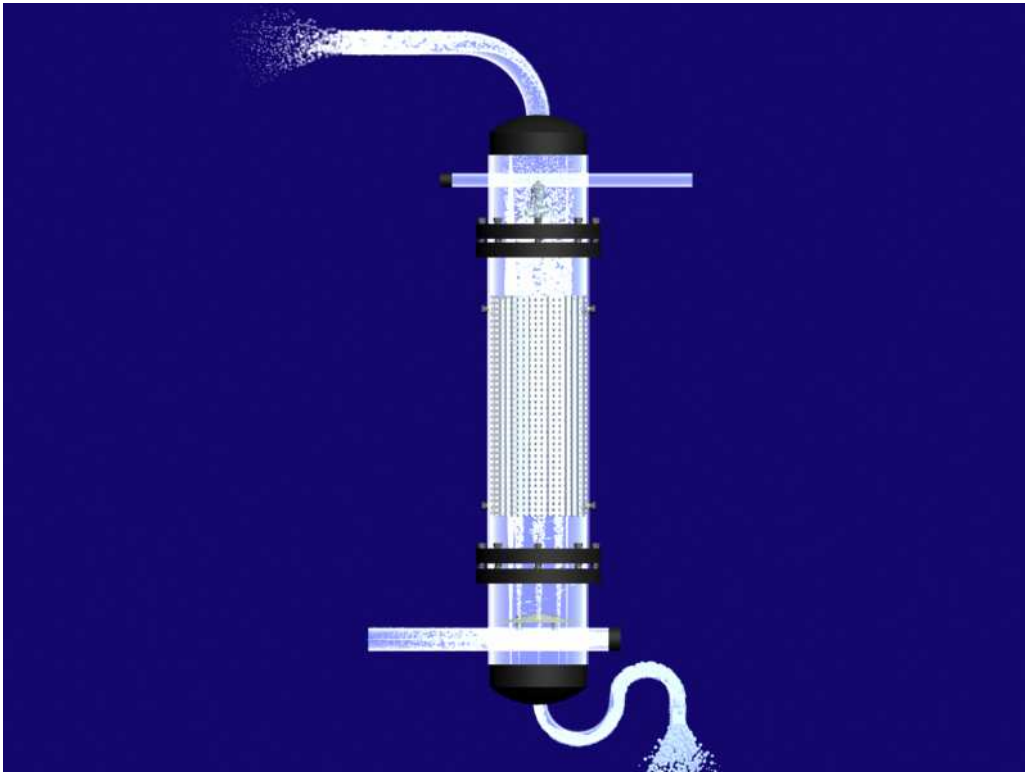ates up to 30 m (1 ft) of packing material along the length. The two towers are connected by two 25.4 cm (10" nominal) ID PVC elbows which provide sufficient space for both holding drain water and providing an air flow channel.

17	Air inlet port	11	Packing material	05	Humidity test port
16	SC water exit port	10	Acrylic Wall	04	Drain port
15	Water inlet port	09	PVC connection	03	Water level test port
14	Humidity test port	08	Water inlet port	02	Water level test port
13	PVC elbow	07	Top hatch	01	SC water inlet port
12	Bottom flanges	06	Air exhaust port	No.	Device
					Direct contact condenser design
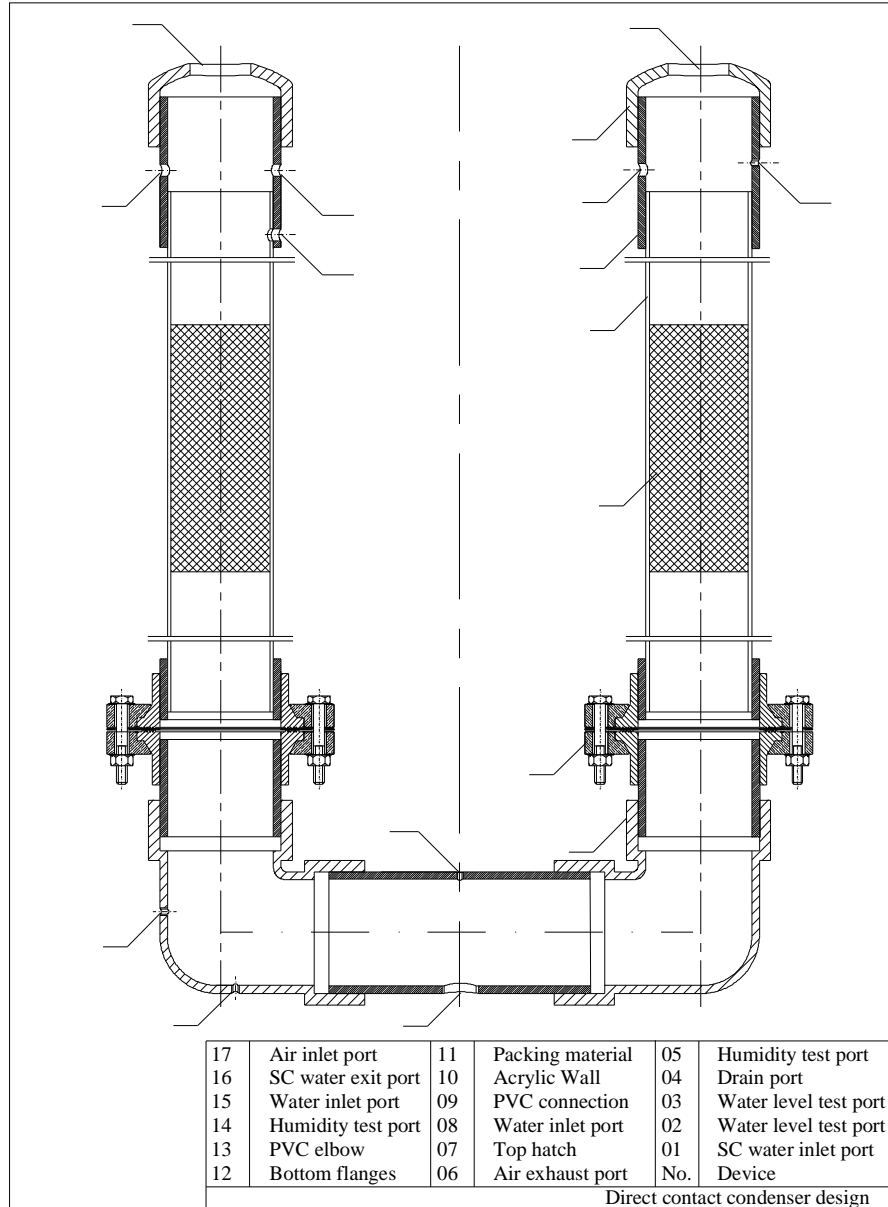
Figure 6 Schematic diagram of experimental direct contact condenser

Water Distributor

     The water distributors for the entire experimental system consist of 3 full cone standard spray nozzles manufactured by Allspray. The three nozzles each maintain a uniform cone angle of 60°. The nozzle is designed to allow a water capacity of about 14.7 lpm, and it is placed more than 50 cm away from the packing material in the diffusion tower to ensure that the spray covers the entire desired area. The spray nozzle pictured in Fig. 7 is a one-piece construction machined from brass bar stock.

Figure 7 Pictorial view of spray nozzle

Pre-heater

     The pre-heater used for the present experiment is a 240 V point source water heater. It possesses a self-contained temperature controller and can deliver water outlet temperatures ranging from 30° to 50° C.

Main Heater

     The main heater consists of two 3 kW electric coil heaters wrapped around a copper pipe through which the feed water flows. The power to the heaters is controlled with two PID feedback temperature controllers with a 240 V output. The feedback temperature to the controllers is supplied with a type J thermocouple inserted in the feed water flow at the discharge of the heater.

Packing Material

     The packing material used in the initial experiments is HD Q-PAC manufactured by Lantec and is shown pictorially in Fig. 8. The HD Q-PAC, constructed from polyethylene, was specially cut using a hotwire so that it fits tightly into the main body of the diffusion tower. The specific area of the packing is 267 m^2/m^3 and its effective diameter for modeling purposes is 1 cm.

Figure 8 Pictorial view of packing matrix

Water Mass Flow Meter

The vane-type water mass flow meter, constructed by Erdco Corporation, has a range of 1.5-15.14 lpm. It has been calibrated using the catch and weigh method. The flow meter has a 4 to 20 mA output that is proportional to flow rate and has an uncertainty of $\pm$ 1% of the full scale.

The turbine water flow meters, constructed by Proteus Industries Inc., have a range of 1.5-12 gpm. They are also calibrated using the catch and weigh method. These flow meters have a 0 to 20 mA or 0-5 V output that is proportional to flow rate, and an uncertainty of $\pm$ 1.5% of the full scale.

Air Mass Flow Meter

The air mass flow rate is measured with a model 620S smart insertion thermal mass flow meter. The flow meter has a response time of 200 ms with changes in mass flow rate. The mass flow meter has a microprocessor-based transmitter that provides a 0-10 V output signal. The mass flow meter electronics are mounted in a NEMA 4X

housing. The meter range is 0-1125 SCFM of air at 25°C and 1 atm (14 PSIG). The uncertainty of the flow meter is ± 1% Full scale + 0.5 % Reading.

Relative Humidity

The relative humidity is measured with two duct-mounted HMD70Y resistance-type humidity and temperature transmitters manufactured by Vaisala Corp. The humidity and temperature transmitters have a 0-10 V output signal and have been factory calibrated.

Temperature and Pressure

All temperature measurements used in the thermal analysis are measured with type E thermocouples. The pressures at the inlet and exit of the diffusion tower are measured with two Validyne P2 static pressure transducers. All of the wetted parts are constructed with stainless steel. The transducers have an operating range of 0-.34 atm (0-5 psi) and have a 0-5 VDC proportional output. The transducers have an accuracy of 0.25% of full scale. They are shock resistant and operate in environments ranging in temperature from –20° to 80° C.

The pressure drop across the test section is measured with a DP15 magnetic reluctance differential pressure transducer. The pressure transducer signal is conditioned with a Validyne carrier demodulator. The carrier demodulator produces a 0-10 VDC output signal that is proportional to the differential pressure. The measurement uncertainty is ± 0.25% of full scale.

Data Collection Facility

A digital data acquisition facility has been developed for measuring the output of the instrumentation on the experimental facility. The data acquisition system consists of a 16-bit analog to digital converter and a multiplexer card with programmable gain manufactured by Computer Boards calibrated for type J thermocouples and 0-10V input ranges. A software package, SoftWIRE, which operates in conjunction with MS Visual Basic, allows a user defined graphical interface to be specified specifically for the experiment. SoftWIRE also allows the data to be immediately sent to an Excel spreadsheet. An example program layout using SoftWIRE is shown in Fig. 9.
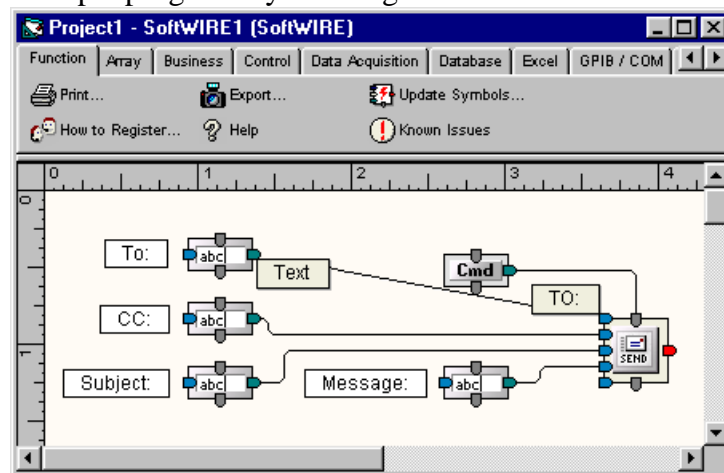

Figure 9 Example program of SoftWIRE

The experimental data acquisition system is designed by using the Virtual Instrumentation module. The control and observation panels are shown in Fig. 10-12. On the "Main" panel, shown in Fig. 10, there is a switch button to begin or stop the data acquisition program. Once the program begins, the experimental data will be recorded in a database file. The file's name, destination and recording frequency can be defined on this panel. Also, all of the experimental measurements are displayed here in real time.
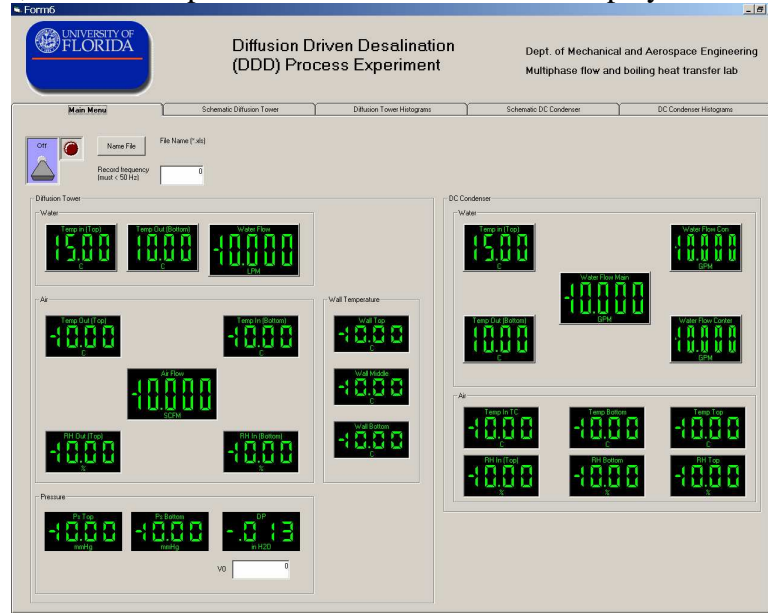
Figure 10 "Main" panel of the DDD data acquisition program

This program also supplies the schematic view panels for the diffusion tower and direct contact condenser, shown in Fig. 11. It shows the position and values of all the measurements from the experimental facility so that the operator can easily control the fresh water production.
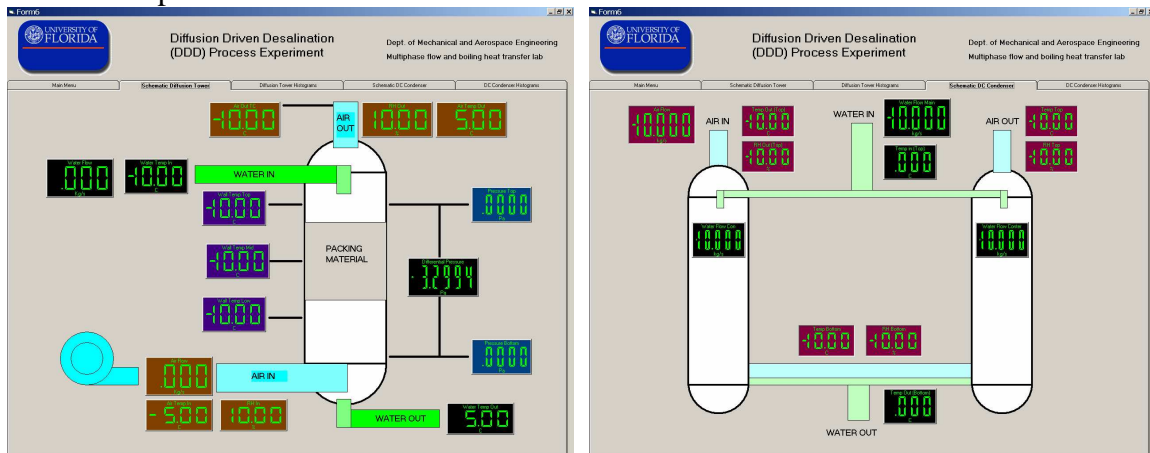
Figure 11 "Schematic view" panels of the DDD data acquisition program

Because the latest research investigation focuses on steady-state operation it is important to know when the physical processes have reached steady-state. The "Histogram View" panels, shown in Fig. 12, are used to display the measurement

variations with time. The x-axis is the time coordinate and y-axis displays the measurement value. The measurement range shown on the y-axis can be changed manually at any time during the experiment to accurately observe the parametric trend.
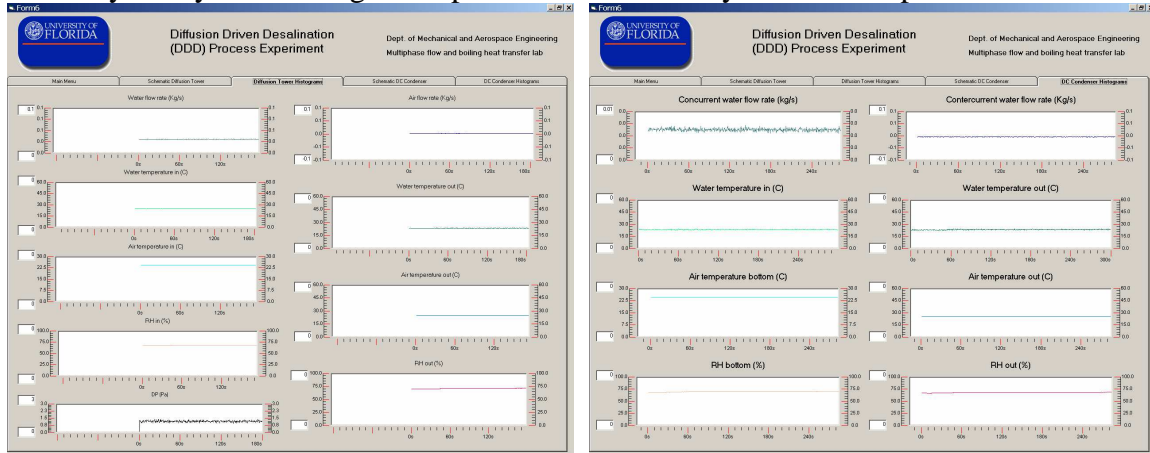
Figure 12 "Histogram view" panels of the DDD data acquisition program

Ion Chromatograph

One objective of the experimental facility is to quantify the purity of fresh water produced with the DDD facility. For this purpose a Dionex ICS-90 isochromatic ion chromatograph has been installed in the Multiphase Heat Transfer and Fluid Dynamics laboratory. The ICS-90 is capable of measuring mineral concentrations down to several parts per billion.

3. Heat and Mass Transfer for the Diffusion Tower

The evaporation of mineralized water in the diffusion tower, shown in Fig. 13, is achieved by spraying heated feed water on top of a packed bed and blowing the dry air counter currently through the bed. The falling liquid will form a thin film over the packing material while in contact with the low humidity turbulent air stream. Heat and mass transfer principles govern the evaporation of the water and the humidification of the air stream. When the system is operating at design conditions, the exit air stream humidity ratio should be as high as possible. The ideal state of the exit air/vapor stream from the diffusion tower is saturated.
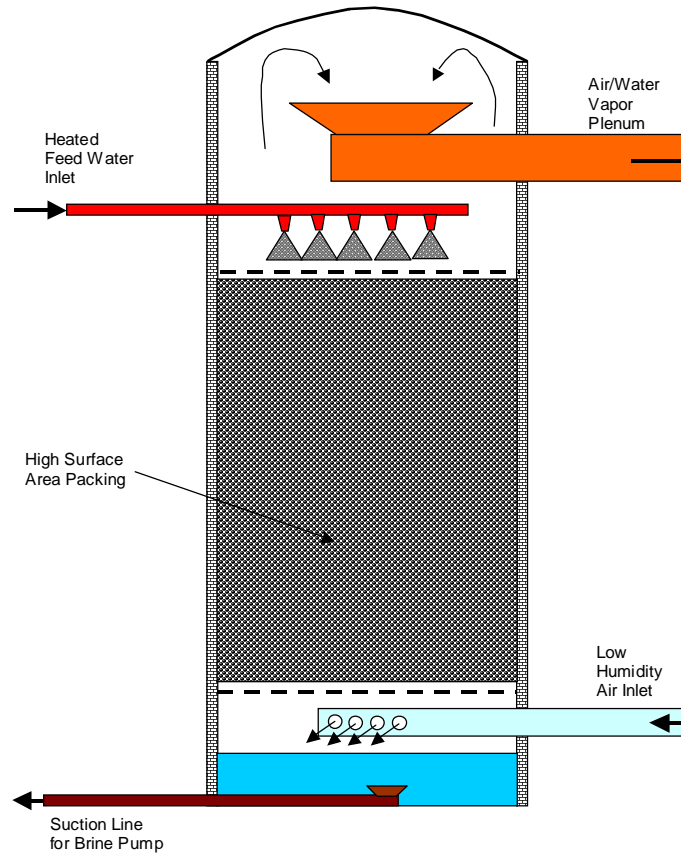
Figure 13 Diagram of diffusion tower

3.1 Heat and Mass Transfer Model for the Diffusion Tower

The most widely used model to estimate the heat and mass transfer associated with air/water evaporating systems is, that due to Merkel [12], which is used to analyze cooling towers. However Merkel's analysis contains two restrictive assumptions,

1) On the water side, the mass loss by evaporation of water is negligible and
2) The Lewis number is unity.

Merkel's analysis is known to under-predict the required cooling tower volume and is not useful for the current analysis since the purpose of the diffusion tower is to maximize the evaporation of water for desalination. Baker and Shryock [13] have presented a detailed analysis of Merkel's original work and have elucidated the error contributed from specific assumptions. Sutherland [14], Osterle [15], and El-Dessouky et al. [16] have presented improved analyses for counter flow cooling towers, yet they inherently contain simplifications that diminish the rigor.

16

Figure 14 Differential control volume for liquid/vapor heat and mass transfer within diffusion tower

The current formulation is based on a two-fluid film model in which conservation equations for mass and energy are applied to a differential control volume shown in Fig.14. The conservation of mass applied to the liquid phase of the control volume in Fig. 14 results in,
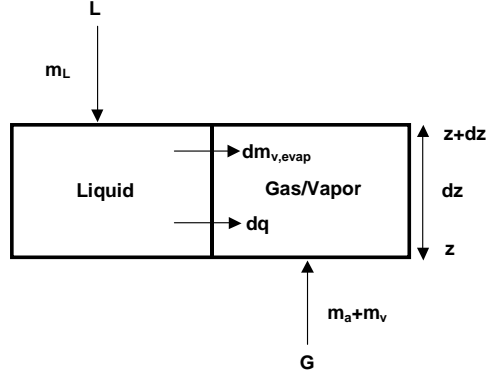
$$\frac{d}{dz}(m_{L,z}) = \frac{d}{dz}(m_{V,evap}),$$ (1)

where m is the mass flow rate, the subscript L denotes the liquid, v denotes the vapor, and evap denotes the portion of liquid evaporated. Likewise, the conservation of mass applied to the gas (air/vapor mixture) side is expressed as,

$$\frac{d}{dz}(m_{V,z}) = \frac{d}{dz}(m_{V,evap}).$$ (2)

For an air/water-vapor mixture the humidity ratio ω, is related to the relative humidity, Φ, through,

$$\omega = \frac{m_V}{m_a} = \frac{0.622\Phi P_{sat}(T_a)}{P - \Phi P_{sat}(T_a)},$$ (3)

where P is the total system pressure and $P_{sat}(T_a)$ is the water saturation pressure corresponding to the air temperature T_a. Using the definition of the mass transfer coefficient applied to the differential control volume in conjunction with the perfect gas law, the gradient of the evaporation rate is expressed as,

$$\frac{d}{dz}(m_{V,evap}) = k_G a_w \frac{M_V}{R}(\frac{P_{sat}(T_i)}{T_i} - \frac{\Phi P_{sat}(T_a)}{T_a})A,$$ (4)

where k_G is the mass transfer coefficient on gas side, a is the specific area of the packing material, a_w is the wetted specific area, M_V is the vapor molecular weight, R is the universal gas constant, T_i is the liquid/vapor interfacial temperature and A is the cross sectional area of the diffusion tower. Combining Eqs. (2), (3), and (4) the gradient of the humidity ratio in the diffusion tower is expressed as,

$$\frac{d\omega}{dz} = \frac{k_G a}{G} \frac{M_V}{R}(\frac{P_{sat}(T_i)}{T_i} - \frac{\omega}{0.622 + \omega}\frac{P}{T_a}),$$ (5)

where $G = \frac{m_a}{A}$ is the air mass flux. Equation (5) is a first order ordinary differential equation with dependent variable, ω, and when solved yields the variation of humidity

ratio along the length of the diffusion tower. In order to evaluate the liquid/vapor interfacial temperature it is recognized that the energy convected from the liquid is the same as that convected to the gas,

$$U_L(T_L - T_i) = U_G(T_i - T_a),\tag{6}$$

where U_L and U_G are the respective liquid and gas heat transfer coefficients, and the interfacial temperature is evaluated from,

$$T_i = \frac{T_L - {U_G}/{U_L}\,T_a}{1 + {U_G}/{U_L}}.\tag{7}$$

In general the liquid side heat transfer coefficient is much greater than that on the gas side, thus the interfacial temperature is only slightly less than that of the liquid.

The conservation of energy applied to the liquid phase of the control volume yields,

$$\frac{d}{dz}(m_L h_L) = \frac{d(m_{V,evap})}{dz}h_{Fg} + Ua(T_L - T_a)A,\tag{8}$$

where U is the overall heat transfer coefficient and h is the enthalpy. Noting that $dh_L = C_{p_L}dT_L$ and combining with Eqs. (8) and (1) results in an expression for the gradient of water temperature in the diffusion tower,

$$\frac{dT_L}{dz} = \frac{G}{L}\frac{d\omega}{dz}\frac{(h_{Fg} - h_L)}{C_{p_L}} + \frac{Ua(T_L - T_a)}{C_{p_L}L},\tag{9}$$

where L= $\dfrac{m_L}{A}$ is the water mass flux. Equation (9) is also a first order ordinary differential equation with T_L being the dependent variable and when solved yields the water temperature distribution through the diffusion tower.

The conservation of energy applied to the air/water-vapor phase of the control volume yields,

$$-\frac{d}{dz}(m_a h_a + m_V h_V) + \frac{d(m_{V,evap})}{dz}h_{Fg} =$$
$$-Ua(T_L - T_a)A.\tag{10}$$

Noting that the specific heat of the air/vapor mixture is evaluated as,

$$C_{p_{mix}} = \frac{m_a}{m_a + m_V}C_{Pa} + \frac{m_V}{m_a + m_V}C_{pV},\tag{11}$$

and combining with Eqs. (10) and (2) yields the gradient of air temperature in the diffusion tower,

$$\frac{dT_a}{dz} = -\frac{1}{1+\omega}\frac{d\omega}{dz}\frac{h_L(T_a)}{C_{p_{mix}}} + \frac{Ua(T_L - T_a)}{C_{p_{mix}}G(1+\omega)}.\tag{12}$$

Equation (12) is also a first order ordinary differential equation with T_a being the dependent variable and when solved yields the air/vapor mixture temperature distribution along the height of the diffusion tower.

Equations (5), (9), and (12) comprise a set of coupled ordinary differential equations that are used to solve for the humidity ratio, water temperature, and air/vapor mixture temperature distributions along the height of the diffusion tower. However, since a one-dimensional formulation is used, these equations require closure relationships. Specifically, the overall heat transfer coefficient and the gas side mass transfer coefficient

are required. A significant difficulty that has been encountered in this analysis is that correlations for the water and air/vapor heat transfer coefficients for film flow though a packed bed, available in the open literature (McAdams et al. [17] and Huang and Fair [18]), are presented in dimensional form. Such correlations are not useful for the present analysis since a special matrix type packing material is utilized, and the assumption employed to evaluate those heat transfer coefficients are questionable. In order to overcome this difficulty the mass transfer coefficients are evaluated for the liquid and gas flow using a widely tested correlation and a heat and mass transfer analogy is used to evaluate the heat transfer coefficients. This overcomes the difficulty that gas and liquid heat transfer coefficients cannot be directly measured because the interfacial film temperature is not known.

The mass transfer coefficients associated with film flow in packed beds have been widely investigated. The most widely used and perhaps most reliable correlation is that proposed by Onda et al. [19]. Onda's correlation, shown in Appendix A, is used to calculate the mass transfer coefficients in the diffusion tower, k_G and k_L. However, it was found at Onda's correlation under-predicted the wetted specific area of the packing material. Therefore, a correction was made as follows,

$$a_w = a\left\{1 - \exp\left[-2.2\left(\frac{\sigma_c}{\sigma_L}\right)^{3/4} \text{Re}_{LA}^{1/2} Fr_L^{-0.05} We_L^{1/5}\right]\right\}, \tag{13}$$

See Appendix A for details.

As mentioned previously, the heat and mass transfer analogy is used to compute the heat transfer coefficients for the liquid side and the gas side. Therefore the heat transfer coefficients are computed as follows,

heat transfer coefficient on the liquid side

$$\frac{Nu_L}{\text{Pr}_L^{1/2}} = \frac{Sh_L}{Sc_L^{1/2}}, \tag{14}$$

$$U_L = k_L(\rho_L C_{PL} \frac{K_L}{D_L})^{1/2}, \tag{15}$$

heat transfer coefficient on the gas side

$$\frac{Nu_G}{\text{Pr}_G^{1/3}} = \frac{Sh_G}{Sc_G^{1/3}}, \tag{16}$$

$$U_G = k_G(\rho_G C_{PG})^{1/3}(\frac{K_G}{D_G})^{2/3}, \tag{17}$$

overall heat transfer coefficient

$$U = (U_L^{-1} + U_G^{-1})^{-1}, \tag{18}$$

where K denotes thermal conductivity and D denotes the molecular diffusion coefficient.

In order to test the proposed heat and mass transfer model, consideration is first given to the cooling data of McAdams et al. [17]. The data shown are for air water counter current flow in a 15.24 cm bed packed with 2.54 cm carbon Raschig rings. Using the analysis presented above, the exit water temperature, exit air temperature, and exit humidity ratio are computed using the following procedure: 1) guess the exit water temperature; 2) compute the temperature distributions and humidity distribution through

the packed bed using Eqs. (5), (9), and (12); 3) Check whether the predicted inlet water temperature agrees with the measured inlet water temperature, and stop the computation if agreement is found, otherwise repeat the procedure from step 1. A comparison between the measured exit water temperature, exit air temperature, and exit humidity ratio reported by McAdams et al. with those computed using the current model are shown in Figs. 15 a and b. As seen in the figures the comparison is generally good. The exit air temperature and exit humidity ratio are slightly under-predicted. The exit water temperature is slightly over-predicted. It is noted that McAdams et al. were not confident with the humidity measurement, and there is some error in the measurement because when the humidity ratio is converted to relative humidity for some data, the computed values exceed 100%. The actual humidity should lie closer to the predicted values.
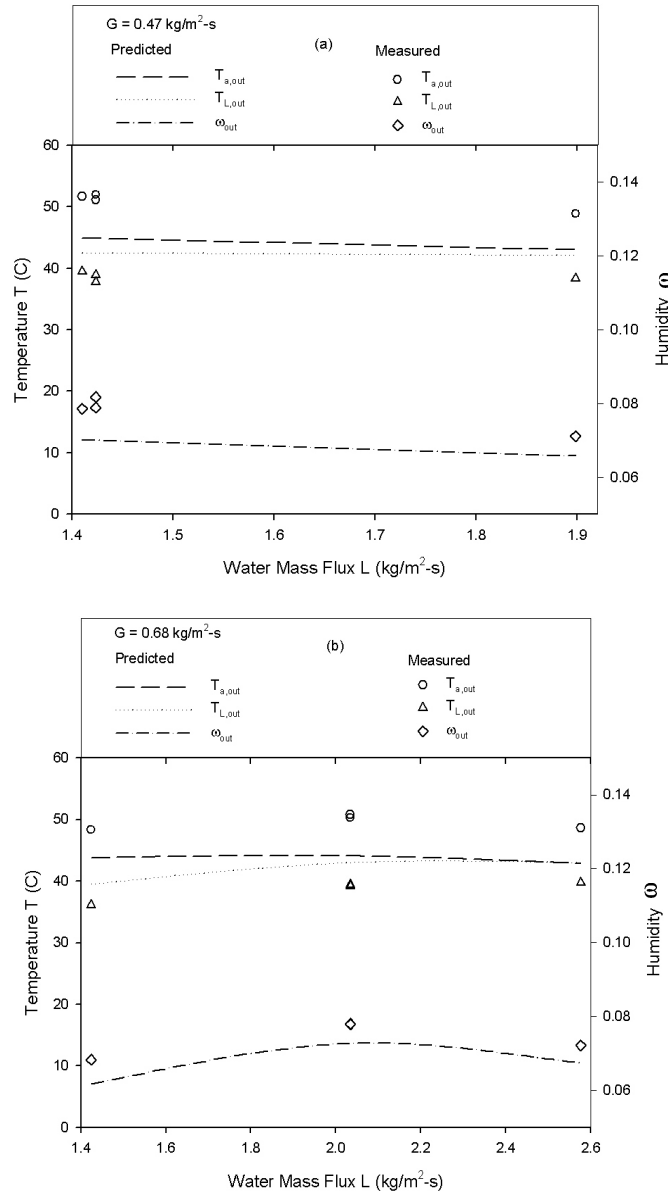
Figure 15 Comparison of predicted exit conditions with the data of McAdams et al. [17]

20

3.2 Operating Performance

Heat and mass transfer experiments were carried out in the diffusion tower with a packing bed height of 20 cm. The liquid mass flux was fixed at 1.75, 1.3, and 0.9 kg/m^2-s and the air mass flux was varied from about 0.6-2.2 kg/m^2-s. The inlet air temperature was about 23° C while the inlet water temperature was 60° C. The experiments were repeated to verify the repeatability of the results. The measured exit humidity, exit air temperature, and exit water temperature are compared with those predicted with the model for all three different liquid mass fluxes in Figs. 16 a-c. It is observed that the repeatability of the experiments is excellent, and so is the comparison between the predicted and measured exit water temperature and exit humidity ratio. The exit air temperature is slightly over predicted.
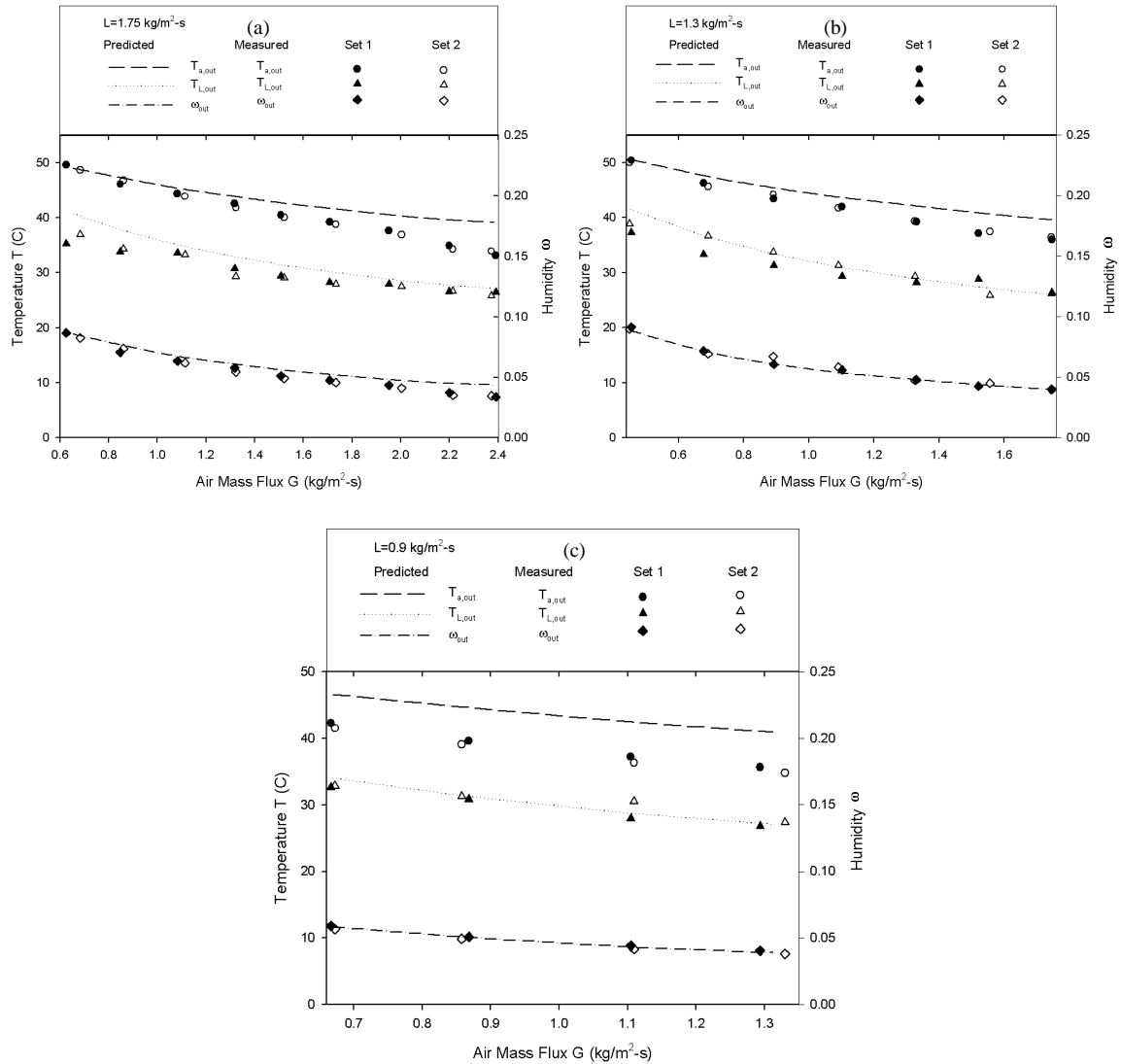
Figure 16 Comparison of predicted exit conditions with the experimental data for different liquid mass fluxes, L= a) 1.75, b) 1.3, and c) 0.9 kg/m^2-s.

In general, the analytical model proves to be quite satisfactory in predicting the thermal performance of counter flow packed beds. The excellent agreement of the model with the measured exit water temperature and exit humidity ratio is most important for desalination and water-cooling applications. A rigorous set of conservation equations have been developed for a two-fluid model and mass transfer closure has been achieved using a widely tested empirical correlation, while heat transfer closure has been achieved by recognizing the analogous behavior between heat and mass transfer. The model does not require questionable assumptions that have plagued prior analyses. It is believed that the current model will be very useful to both designers of diffusion towers for desalination applications as well as designers of cooling towers for heat transfer applications.

3.3 Pressure Drop through the Packing Material

The pressure drop through the packing material on the air side influences the energy consumption prediction of the DDD process. Therefore experiments considering the air pressure drop with water loading is another important objective in the research. This experiment is executed without heating the water. The comparison of the predicted pressure drop and the experimental data are shown below in Fig. 17 for different water mass flux loadings.
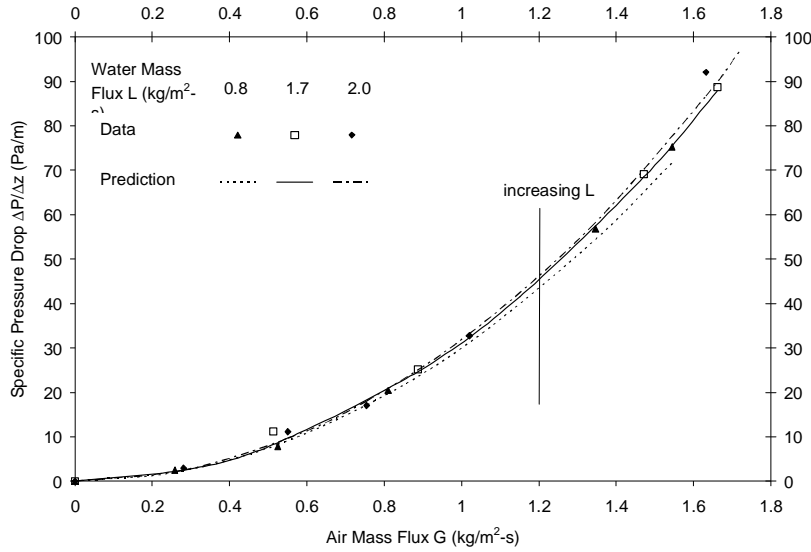
Figure 17 Air specific pressure drop variation with air mass flux for water mass flux L

The pressure drop is predicted using the empirical correlation specified by the manufacturer of the packing material. Figure 17 clearly shows that the pressure drop correlation is accurate for HD Q-Pac packing material. Another interesting result is that the air specific pressure drop increases with increasing water mass flow rate under the same air mass flow rate. The air side dimensional pressure drop correlation is:

$$\frac{\Delta P}{z} = \rho_G V_G^2 (3.54 \times 10^{-5} + 0.654 V_L^2 + 1.176 \times 10^4 V_L^4 \rho_G^2 V_G^4) \quad \textbf{(19)}$$

where z is the height of the packing material (m), ΔP is the pressure drop through the packing (Pa), ρ_G is the gas density (kg/m^3), V_G is the superficial gas velocity through the packing (m/s), and V_L' is the superficial liquid velocity through the packing (m/s).

Using π-theory, the following dimensionless variables are identified as being important to the pressure drop: $Eu_G = \dfrac{\Delta P}{\rho_G V_G^2}$, $\mathrm{Re}_{GD} = \dfrac{\rho_G V_G D}{\mu_G}$, $\mathrm{Re}_{LD} = \dfrac{\rho_L V_L D}{\mu_L}$ and $\varepsilon = \dfrac{D}{z}$. Equation (19) may be rearranged as,

$$Eu_G \varepsilon = C_1 + C_2 \, \mathrm{Re}_{LD}^2 + C_3 \, \mathrm{Re}_{LD}^4 \, \mathrm{Re}_{GD}^4 \tag{20}$$

$$C_1 = 3.54 \times 10^{-5} D \tag{21}$$

$$C_2 = 0.654 \frac{\mu_L^2}{\rho_L^2 D} \tag{22}$$

$$C_3 = 1.176 \times 10^4 \frac{\mu_L^4 \mu_G^4}{\rho_L^4 \rho_G^2 D^7} \tag{23}$$

where D is the cross section diameter of the packing (m), ρ_L is the liquid density (kg/m^3), μ_L is liquid viscosity (Pa-s), μ_G is gas viscosity (Pa-s). Although the constants in Eqn. (21) - (23) are dimensional, Eqn. (20) elucidates the dimensionless variables that control pressure drop through packed bed.

4. Direct Contact Condenser Heat and Mass Transfer

4.1 Outline of Direct Contact Condensation Modeling Effort

To develop an effective design and reliable heat transfer model for the direct contact condenser, one-dimensional mass, momentum, and energy transfer conservation between the phases is considered. The 1-D model is based on the conservation principles with the assumption of a uniform cross-section. Furthermore, the motion of droplets is modeled using a continuum approach so that it is consistent with the gas phase. The analysis presented below is applicable to a spray-type direct contact condenser without packing.

Variation of droplet size—mass transfer
The physical model concerned in this spray-type direct contact condenser simulation is shown in Fig. 18.
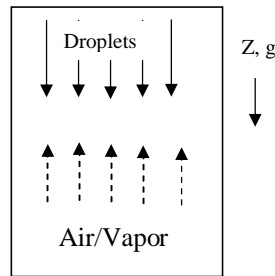

Figure 18 Physical model diagram of the spray-type direct contact condenser

The cold fresh-water droplets at temperature T_d will increase in size due to the condensation of the vapor, which is contain ed in the gas stream at a higher temperature T_a. The rate of change in the droplet radius, R_d, as it flows down the condenser chamber can be computed as

$$\frac{dR_d}{dz} = \gamma_d \frac{[\rho_v(T_a) - \rho_{sat}(T_d)]}{\rho_w v_d} \tag{24}$$

where z is the vertical coordinate, as shown in the above control volume, measuring from where droplets are introduced, and the mass transfer coefficient γ_d is empirically calculated from

$$\gamma_d = \frac{D(2 + 0.5\,\mathrm{Re}^{1/2})}{2R_d} \tag{25}$$

in which D is the diffusion coefficient and Reynolds number is based on the relative velocity between the droplet, $v_d(z)$, and gas/vapor velocity, $u(z)$, as

$$\mathrm{Re} = \frac{2\rho_a R_d |v_d(z) - u(z)|}{\mu_a}.$$

Droplet velocity/trajectory – momentum transfer

To predict the droplet velocity $v_d(z)$, Newton's 2nd law is applied,

$$\frac{dv}{dz} = \frac{g}{v_d(z)} - C_{drag}\frac{\rho_a[v_d(z) - u(z)]^2}{2v_d(z)}\frac{\pi R_d^2}{m_{drop}} \tag{26}$$

where $C_{drag} = \frac{24}{\mathrm{Re}}\left(1 + \frac{1}{6}\mathrm{Re}^{2/3}\right)$ is the aerodynamic drag on the droplet based on a standard empirical correlation, $m_{drop} = (4/3)\pi R_d^3 \rho_l$ is the mass of an individual droplet, and g is the gravitational acceleration.

Droplet temperature – energy transfer

The droplet temperature is affected by the convective heat transfer of the air/vapor flow around the droplet and the phase change. It can be computed as,

$$\frac{dT_d}{dz} = \frac{3\{U[T_a(z) - T_d(z)] + \gamma_d(h_{fg}(z) - C_p T_d)(\rho_v(T_a) - \rho_{sat}(T_d))\}}{C_{pl}\rho_l R_d v_d} \tag{27}$$

where U is the heat transfer coefficient that depends on Re, h_{fg} is the latent heat, ρ_l is water density, and ρ_{sat} is vapor saturation density.

Air temperature variation– energy transfer

Similarly, the air/vapor temperature can be computed as,

$$\frac{dT_a}{dz} = \frac{4\pi R_d^2 Nu_d \{U[T_a(z) - T_d(z)]\}}{\rho_a C_{pa}(v_d(z) - u(z))} \tag{28}$$

where Nu_d is the Nusselt number.

Change in the water vapor density—mass transfer

The water vapor density decreases in the condenser due to a drop in the vapor partial pressure via condensation. It can be computed as

$$\frac{d\rho_v}{dz} = \frac{4\pi R_d^2 Nu_d \{\gamma_d [\rho_{sat}(T_d) - \rho_v(z)]\}}{(v_d(z) - u(z))} \tag{29}$$

where the saturation vapor density and relative humidity are related as: $\rho_{sat}(T_a)\Phi = \rho_{sat}(T_d)$.

Boundary conditions

The initial droplet size at top of the condenser is R_{d0} and it is at temperature T_{d0} with an injection velocity v_{d0} at $Z = 0$. At the air/vapor inlet, $Z = H$, the air temperature is T_{a0} and vapor density is ρ_{v0}, which is taken as the saturated vapor density corresponding to air temperature T_a. Hence,

$R_d\big|_{z=0} = R_{d0}; T_d\big|_{z=0} = T_{d0}; v_d\big|_{z=0} = v_{d0}; T_a\big|_{z=H} = T_{aH}; \rho_v\big|_{z=H} = \rho_{vH}$.

Solution Methodology

Equations (24)-(29) comprise a set of coupled ordinary differential equations that are used to solve for the humidity ratio, water temperature, and air/vapor mixture temperature distributions along the height of the condenser. The coupled first order nonlinear ODE's can be easily solved by the shooting method using a simple finite difference scheme with some reasonable initial guesses for the unknowns. The iteration continues until the convergence is reached.

4.2 Condenser Performance

Initially, the steady state heat and mass transfer experiments were carried out in the spray-type direct contact condenser without packing described in section 2.1. The hot saturated air inlet mass flux was fixed at 0.875 kg/m²-s and its inlet temperature was varied from about 37° C to 42° C. The inlet cold fresh water temperature was about 27° C. For a fixed air inlet temperature, a full range of cold water flow rates varying from zero to maximum was explored where steady state conditions were maintained for several distinct flow rates. Thus data of the condenser's performance for several different steady states is obtained. The data are shown in the figures to follow. The experiments were repeated to verify the repeatability of the results. It is observed that the repeatability of the experiments is excellent, and specific trends are clear. There is always a maximum heat and mass transfer condition that is evident in the experiments.

Fig. 19 shows the total temperature drop of the air/vapor mixture as it passes through both the co-current and countercurrent condenser stages. The air temperature drop increases with the water to air mass flow ratio for a certain air inlet temperature. And it also increases with increasing air inlet temperature when the water to air mass flow ratio is fixed. With no water flow, there is a finite temperature drop of the air/vapor

mixture which implies there is a degree of cooling due to heat loss to the environment from the condenser walls. Indeed, for a practical condenser design the heat loss is good since it enhances condensation. The U-shape design of the condenser not only reduces the construction area, but also increases the wall area of the condenser which increases the heat loss of the air. This is demonstrated clearly in the experiments. However, the figure also shows that for a certain air inlet temperature there exists a threshold to air mass flow ratio that yields a maximum temperature drop. Once this threshold is exceeded, the air temperature drop hardly changes with increasing water to air mass flow ratio.

Figure 19 Total temperature drop of the air/vapor mixture with varying water to air mass flow ratios and different air inlet temperatures (without packing)

Fig. 20 shows the total fresh water production rate by both condenser stages. It shows that for a fixed feed water inlet temperature and air inlet mass flux, the fresh water production rate is strongly dependent on both the feed water to air mass flow ratio and the air inlet temperature. Trends show that the fresh water production decreases significantly with a small drop in the air inlet temperature. This trend suggests that there will be little to no fresh water production when the air inlet temperature is lower than 30° C. The peak in temperature drop observed in Fig. 19 results in a peak in fresh water production as shown in Fig. 20. Therefore increasing the water to air mass flow ratio past the threshold does not result in increasing the fresh water production rate.

Figure 20 Total fresh water production rate with varying water to air mass flow ratios and different air inlet temperatures (without packing)

Figs. 21 and 22 show the temperature drop of the air/vapor mixture through the co-current and the countercurrent condenser stages, respectively. The air/vapor mixture's temperature drop shows the same trend in these figures as in Fig. 19. The main difference is that the heat loss in the countercurrent condenser stage is very small because the air/vapor mixture already loses a lot of energy in the co-current stage before it enters the countercurrent condenser stage. The heat transfer driving potential is not large enough to overcome the heat resistance of the condenser wall.
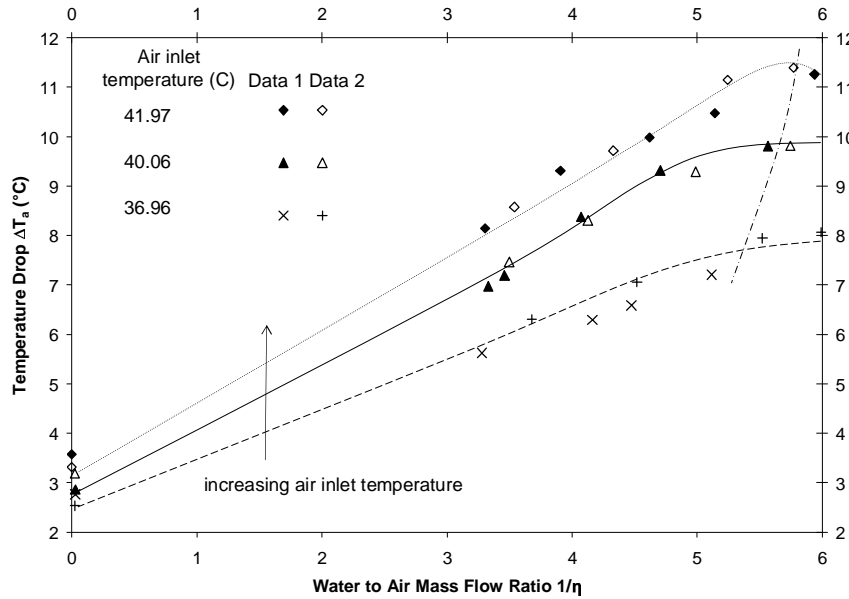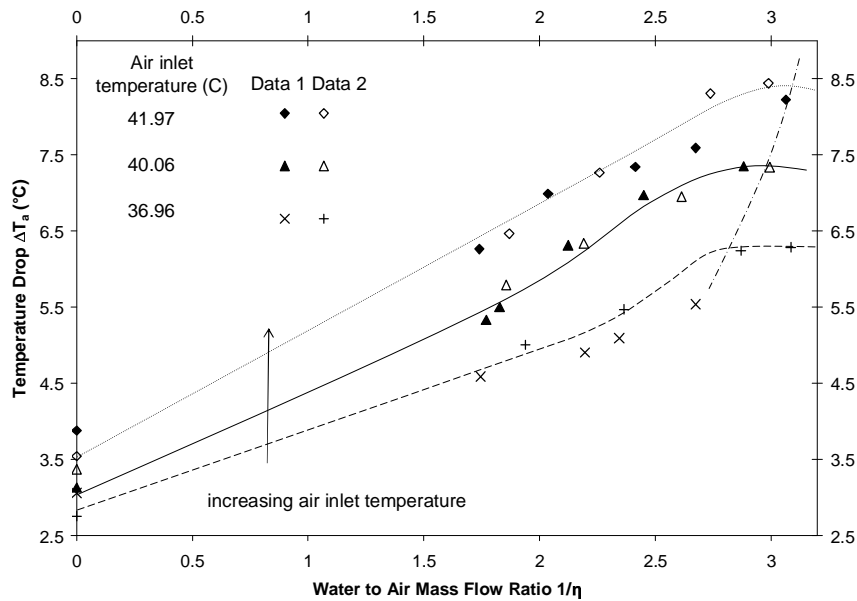

Figure 21 Temperature drop of the air/vapor mixture with varying water to air mass flow ratios in the co-current and different air inlet temperatures stage (without packing)

27
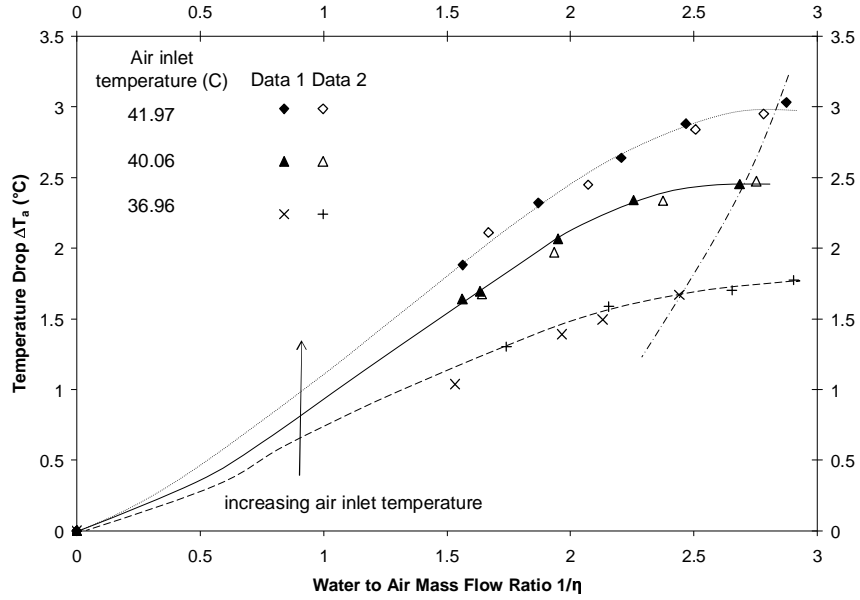
Figure 22 Temperature drop of the air/vapor mixture with varying water to air mass flow ratios in the countercurrent stage (without packing) and different air inlet temperatures

Figs. 23 and 24 show the fresh water production rate through the co-current and the countercurrent condenser stages, respectively. By comparing Fig. 23 and Fig. 24 for the same air inlet temperature, the maximum fresh water production rate in the countercurrent condenser stage is about 25% of that in the co-current stage, which means the countercurrent stage is very important to the total production of the system.

Figure 23 Fresh water production rate with varying water to air mass flow ratios and different air inlet temperatures in the co-current stage (without packing)
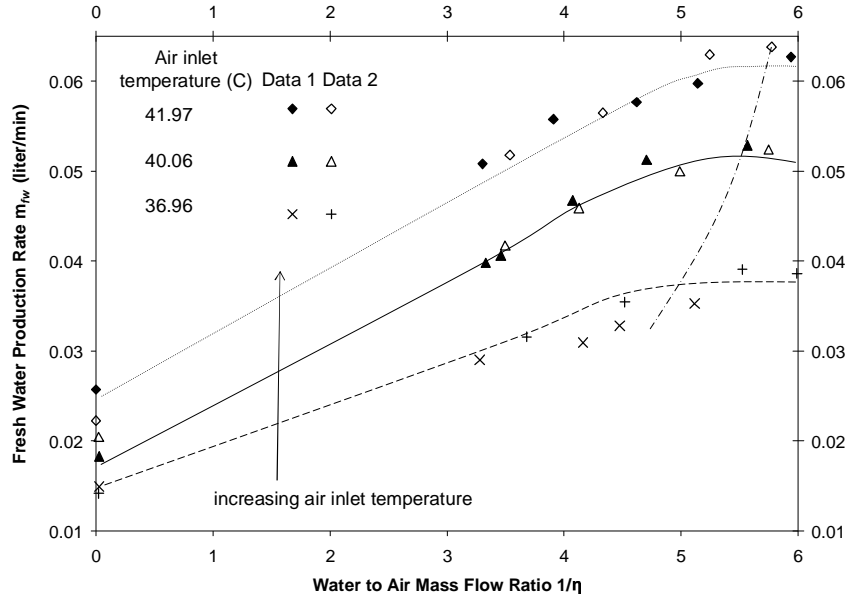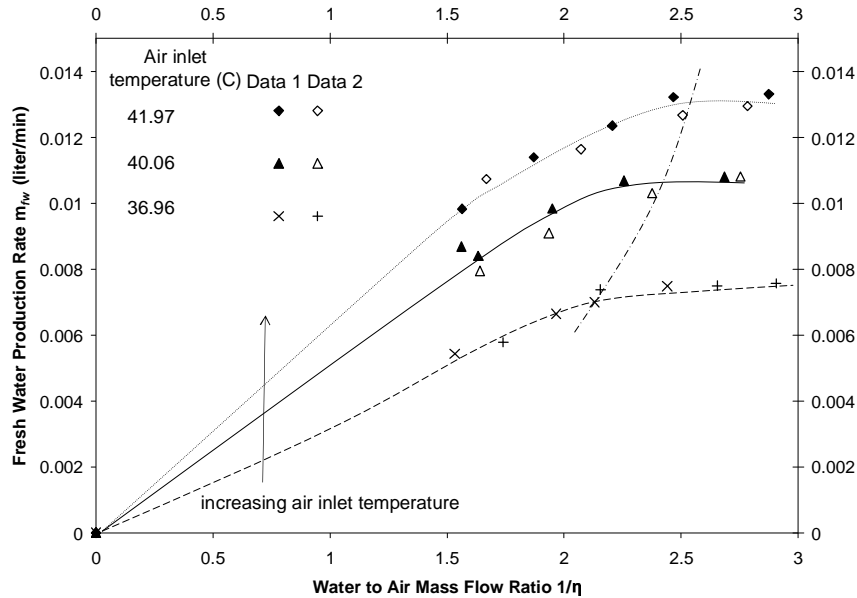
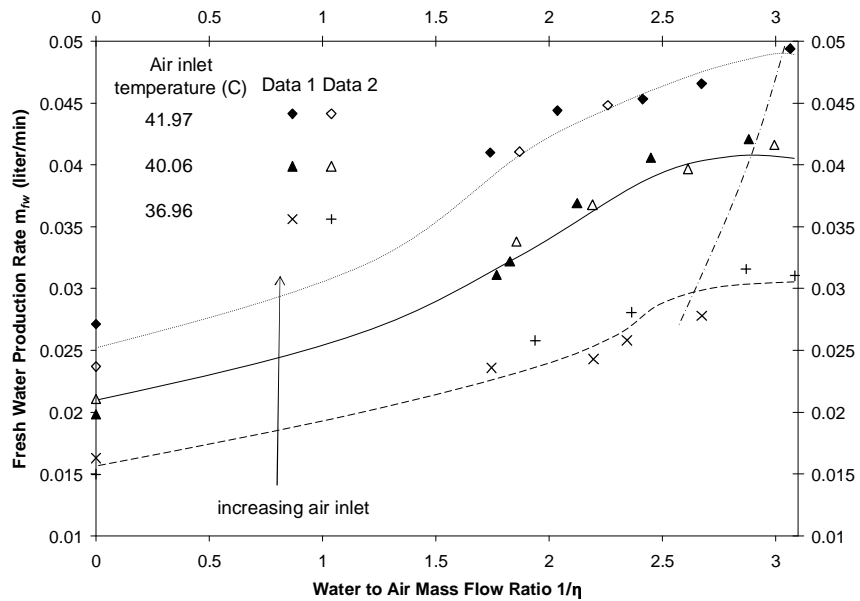Figure 24 Fresh water production rate with varying water to air mass flow ratios and different air inlet temperatures in the countercurrent stage (without packing)

Detailed experimental data associated with Figs. 19-24 are shown in Appendix B. All figures show that there exists a threshold cold water to air mass flow ratio where the air temperature drop and fresh water production rate reach a maximum. When the water to air mass flow ratio increases beyond this threshold, neither the air temperature drop nor the fresh water production rate shows much increase. This interesting phenomenon can be explained by considering the droplet heat transfer process in the condenser. Increasing the cold water flow rate will result in increased droplet velocity and possibly a larger droplet size due to an increased probability of agglomeration. High droplet velocity will reduce the droplet residence time in the condenser which results in reduced heat transfer. Meanwhile, the larger droplet size reduces the heat transfer surface area between the water and air for a given amount of water. Both effects are detrimental to heat transfer. Therefore, as the water to air mass flow ratio is initially increased, an increase in heat transfer is initially observed because the overall surface area for heat transfer is increased with increasing the water to air mass flow ratio. Also the heat capacity is larger and a larger driving potential for heat transfer can be maintained. However, after the threshold is reached, no further increase in heat transfer is observed due to the deleterious effects described above.

Another result shown in the above figures is that the threshold cold water to air mass flow ratio increases with increasing condenser air inlet temperature. For a certain water to air mass flow ratio, hotter saturated air provides a larger driving potential for heat transfer. This larger driving potential overcomes the negative effects of increasing water to air mass flow ratio as described earlier.

The above experiment results suggest that the performance of the spray-type direct contact condenser without packing is not adequate. The size and velocity of the droplets are sufficiently large that the condenser heat transfer performance is less than optimal. In order to overcome this problem, a total of 1.22 m of HD Q-Pac packing

materials are used in the condenser with each condenser stage using 0.61m in each stage to increase the residence time of the cold water. The nozzle in each chamber will spray water on the top of the packing. The air will initially enter the co-current stage. It will flow through the packing in this chamber from top to bottom. Then it will flow into the countercurrent stage and through the packing material upward in this chamber. The droplets will form a liquid film on the surface of the packing material and contact the passing air.

Fig. 25 shows the total temperature drop of the air/vapor mixture as it passes through both the co-current and countercurrent condenser stages. The air temperature drop increases with both increasing water to air mass flow ratio and air inlet temperature. Like the case with no packing there also exists a threshold water to air mass flow ratio beyond which no further increase in temperature drop is observed. By comparing Fig. 19 with Fig. 25, it clearly shows that with packing at the same air inlet temperature and cold water temperature, the maximum air temperature drop increases and the threshold water to air flow ratio is smaller. These results demonstrate condenser improvement with the addition of packing.

Figure 25 Total temperature drop of the air/vapor mixture with varying water to air mass flow ratios and different air inlet temperatures (with packing)

Fig. 26 shows the total fresh water production rate yielded by both condenser stages. It shows that for fixed feed water inlet temperature and air inlet mass flux, the fresh water production rate increases rapidly with both the feed water to air mass flow ratio and the air inlet temperature. As previously discussed, there exists a threshold water to air mass flow ratio beyond which no further increases in production rate are observed.
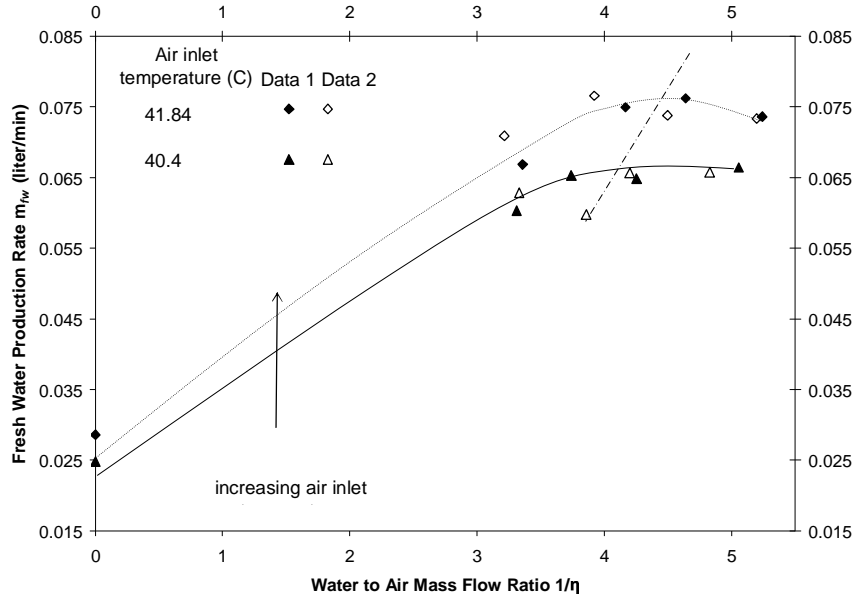
Figure 26 Total fresh water production rate with varying water to air mass flow ratios and different air inlet temperatures (with packing)

Figs. 27 and 28 show the temperature drop of the air/vapor mixture through the co-current and the countercurrent condense stage respectively. Fig. 29 and Fig. 30 show the fresh water product rate through the co-current and the countercurrent condense stage respectively.
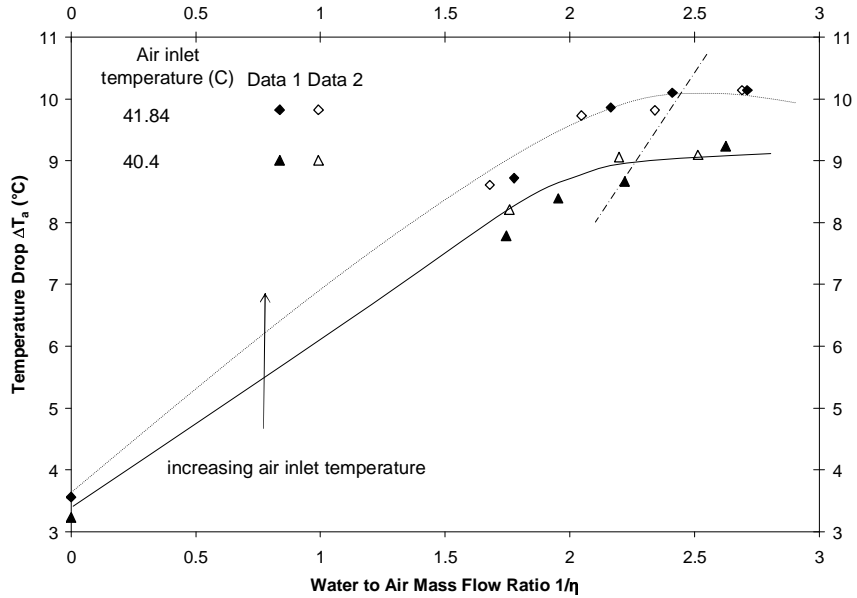
Figure 27 Temperature drop of the air/vapor mixture with varying water to air mass flow ratios and different air inlet temperatures in the co-current stage (with packing)

31
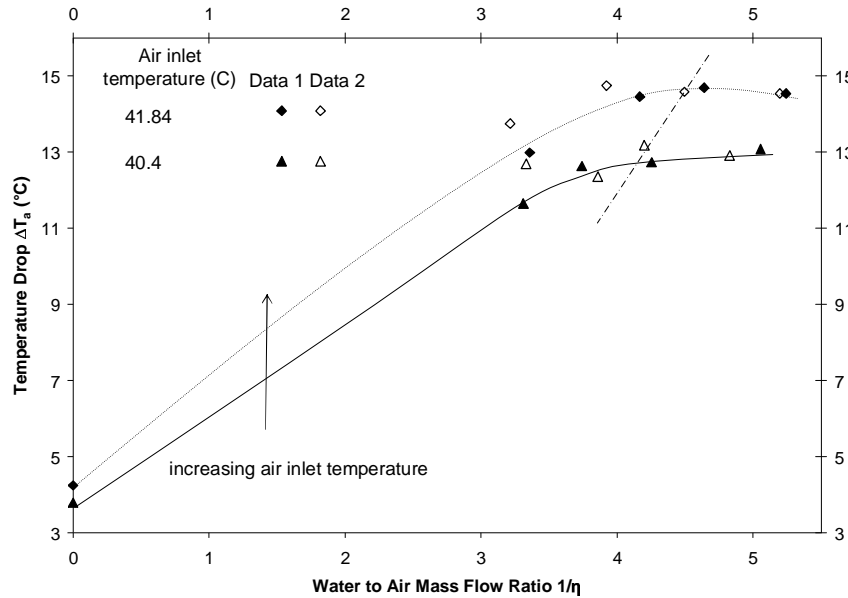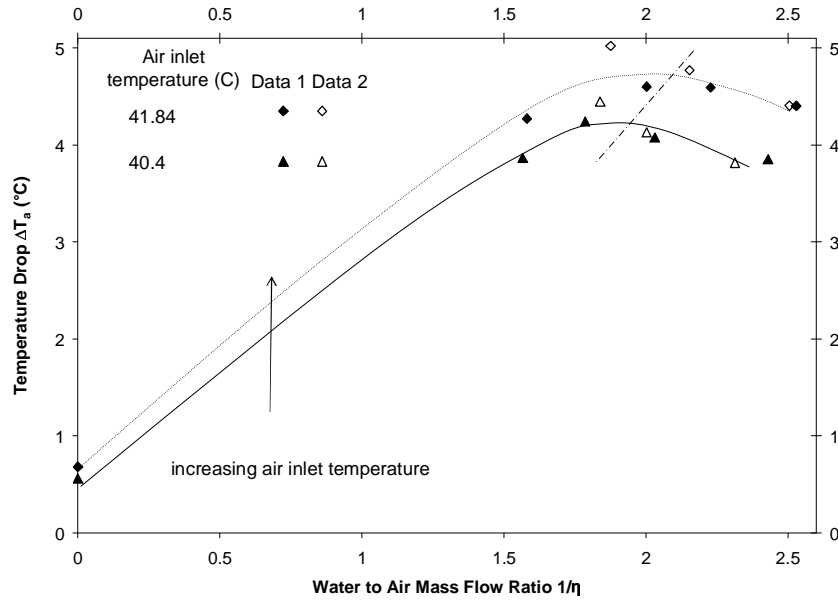
Figure 28 Temperature drop of the air/vapor mixture with varying water to air mass flow ratios and different air inlet temperatures in the countercurrent stage (with packing)
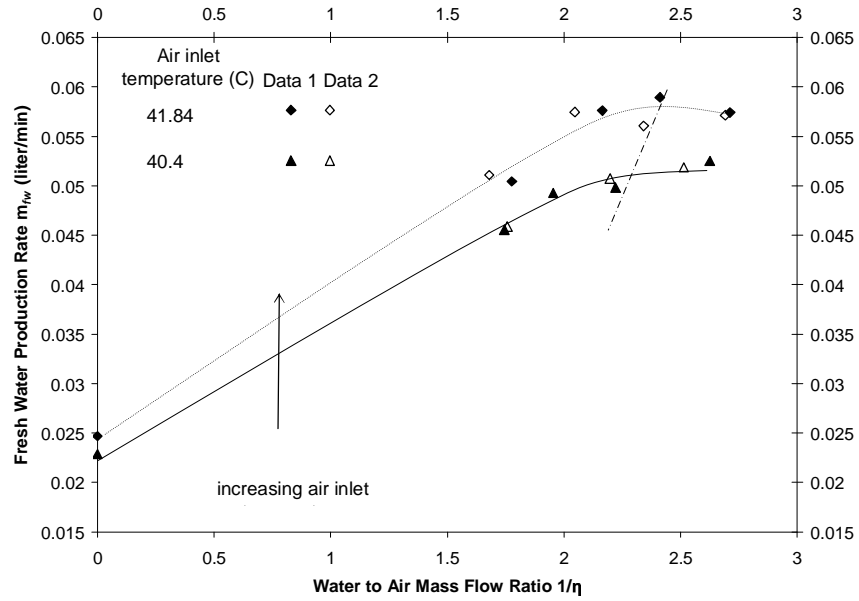
Figure 29 Fresh water production rate with varying water to air mass flow ratios and different air inlet temperatures in the co-current stage (with packing)
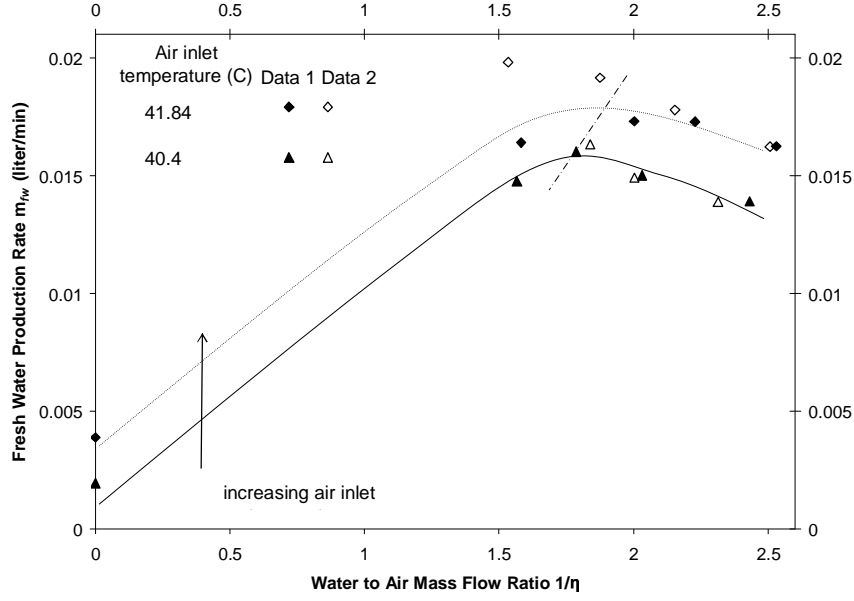
Figure 30 Fresh water production rate with varying water to air mass flow ratios and different air inlet temperatures in the countercurrent stage (with packing)

Detailed experimental data associated with Figs. 25-30 are shown in Appendix C. All figures show that there exists a threshold cold water to air mass flow ratio where the condenser heat transfer is maximum. This phenomenon can be explained by the heat transfer process in the condenser. Increasing the cold water flow rate will increase the heat capacity of the liquid and will sustain a longer driving potential. Meanwhile, increasing the water to air flow rate will result in increased liquid film thickness, which will be detrimental to heat transfer. A threshold of the water to air mass flow ratio exists where the maximum heat transfer rate is established. The experimental results show the threshold cold water to air mass flow ratio increases with increasing condenser air inlet temperature.

With the same air inlet temperature, air mass flow rate and cold water inlet temperature, Table 3 shows the improvement in condenser performance with the addition of packing. On average, the temperature drop of air increases 30%, fresh water production increases 22%, fresh water production efficiency increases 67.14% and cold water usage reduces 28%. Here, the fresh water condenser production efficiency is

defined as $\dfrac{m_{fw,pack}/m_{c,pack}}{m_{fw,nopack}/m_{c,nopack}} - 1$, where m_c is the cold water flow rate through the

condenser (not the seawater flow rate), m_{fw} is the fresh water product rate, the subscript *nopack* implies without packing, while the subscript *pack* implies with packing.

Table 1 Condenser improvement with the addition of packing

Air inlet Temperature (C)		Air Temperature drop	Fresh water production rate	Fresh water condenser production efficiency	Cold water usage
41.85	Co-current	+34.34%	+30.81%	+47.87%	-11.54%
	Countercurrent	+11.67%	+15.54%	+64.19%	-29.63%
	Total	+27.58%	+16.86%	+57.77%	-25.93%
40.25	Co-current	+42.24%	+41.58%	+108.63%	-32.14%
	Countercurrent	+20.2%	+12.26%	+55.92%	-28%
	Total	+33.97%	+25.58%	+76.50%	-28.85%

The condenser's effectiveness is defined as q/q_{max} , where q_{max} (W) is the maximum possible heat transfer by condenser, and q (W) is the real heat transfer by the condenser. When there is no packing material in the condenser, the final exit air temperature cannot be lower than 30 °C with a cold water inlet temperature of 26 °C. The condenser's effectiveness is less than 77%. With the addition of packing, the exit air temperature is 27.4 °C with a cold water inlet temperature of 26.2 °C. The effectiveness of the condenser is approximately 95%. This performance is impressive.

5. Economic Analysis

5.1 Capacity Evaluation of the DDD system

In order to explore the economic benefits of the performance and parametric bounds of the Diffusion Driven Desalination process, hydrodynamic and thermodynamic analyses were performed. In performing the analyses, the following assumptions have been made:
1) The process operates at steady-state conditions.
2) There are no energy losses to the environment from the heat and mass transfer apparatus.
3) Both the air and water vapor may be treated as perfect gases,
4) Changes in kinetic and potential energy are relatively small.
5) The pumping power for water is that which is necessary to overcome gravity (estimating the exact required pumping power would require significant details regarding the construction of the diffusion tower, heat transfer equipment, and the plumbing; these are beyond the scope of the current analysis).
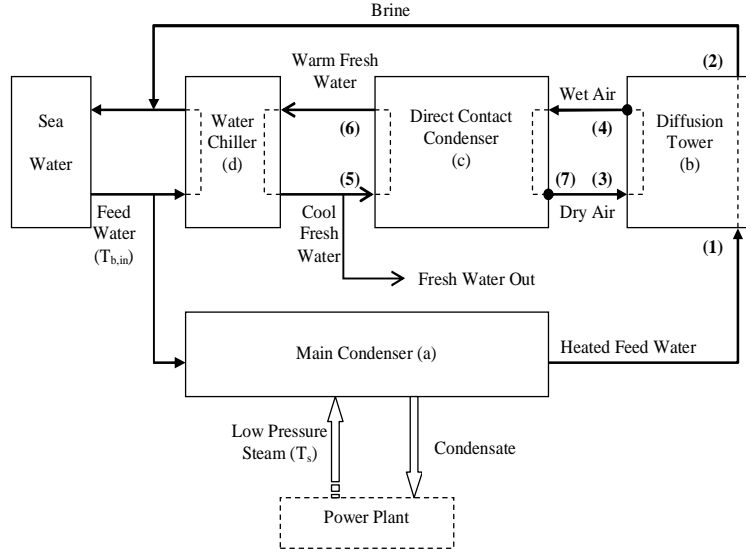
Figure 31 Flow diagram for the DDD process.

A simple flow diagram for the economic analysis of DDD process is shown in Fig. 31. For a fossil fuel power plant with a certain capacity and efficiency, the total input energy and waste heat is,

$$E_{Total} = \frac{E_{elec}}{r} \tag{30}$$

$$E_{waste} = E_{Total} - E_{elec} \tag{31}$$

where E_{elec} (MW) is the capacity of a power plant, r is the energy conversion efficiency, E_{waste} is the waste heat, and E_{Total} is the total input energy. The power plant is assumed to operate with 3" Hg steam pressure in the main condenser. Because the steam is saturated, its temperature $T_{s,in}$ is 46° C. Thus the maximum possible input energy of the DDD process is,

$$E_{DDD} = m_s \lambda \tag{32}$$

where $m_s = \dfrac{E_{waste}}{h_s}$ is the steam mass flow rate in the main condenser, h_s is the steam enthalpy, and λ is the steam latent heat.

In this analysis, it is assumed that a large supply of cool water will be available at a sink temperature, T_L, of 20° C. The condensate in the direct contact condenser will be chilled and a portion of it re-circulated. To avoid providing specifics on the heat transfer equipment, it is assumed that the heat transfer effectiveness in the chiller and condenser is unity, in which $T_L = T_{b,in} = T_5 = T_7 = 20$° C. The temperature of the feed water leaving the main condenser is the high temperature in the system, $T_H = T_{s,in} = T_1 = 46$° C. Using an energy balance in the main condenser, the feed seawater mass flow rate can be calculated as,

$$E_{DDD} = Cp_b m_b (T_1 - T_{b,in}) \tag{33}$$

where m_b is the mass flow rate of the feed water, Cp_b is the average specific heat of the feed water, $T_{b,in}$ is the environmental seawater temperature, and T_1 is the seawater inlet temperature to the diffusion tower.

The air/vapor mixture entering and leaving the diffusion tower is assumed to be fully saturated (relative humidity of unity), and its exit temperature will be predicted from the hydrodynamic model of the diffusion tower. The maximum possible fresh water production exists when the seawater to air mass flow ratio is unity. The fresh water production is expressed as,

$$m_{fw} = m_a \Delta \omega \tag{34}$$

where m_{fw} is the fresh water mass flow rate, ω is the absolute humidity for a certain saturated air temperature, and m_a is the air mass flow rate.

With a known diffusion tower height, the required pumping power on the air and water side can be computed using the diffusion tower analysis described in Section 3.1.

It is also necessary to compute the energy discharge from the direct contact condenser. The exit gas from the diffusion tower is saturated hot air, and discharges in the condenser. The condenser has two primary functions:

1) dehumidify the air to make liquid fresh water,
2) cool the air to the sink temperature so that it can be reused in the diffusion tower.

The total heat removal from the condenser includes heat removal from the vapor and air,

$$E_{DC} = E_v + E_a . \tag{35}$$

On the air side,

$$E_a = Cp_a m_a (T_{a,in} - T_{a,out}) , \tag{36}$$

where Cp_a is the average specific heat of the dry air, $T_{a,in}$ is inlet air temperature to the condenser (T_4), and $T_{a,out}$ is the exit air temperature from the DC condenser (T_7).

On the vapor side, the vapor will release latent heat due to phase change. It will also release heat to the cold fresh water due to the temperature difference, and the total heat release is,

$$E_v = m_v \lambda + Cp_l m_v (T_{l,in} - T_{l,out}) , \tag{37}$$

where $T_{l,in}$ is the inlet vapor temperature of the condenser. $T_{l,in}$ is equal to $T_{a,in}$ (T_4), and $T_{l,out}$ is the exit temperature of the fresh condensate, which is equal to $T_{a,out}$ (T_7). Here, $\dot{m}_v$ is the mass flow rate of the vapor, and Cp_l is the average specific heat of the liquid water.

On the cold fresh water side of the condenser, the water needs to absorb all of the energy released by the air and vapor, and is expressed as

$$E_{DC} = Cp_c m_c (T_{c,out} - T_{c,in}) , \tag{38}$$

where m_c is the mass flow rate of the cold fresh water, Cp_c is the average specific heat, $T_{c,in}$ is the inlet cold fresh water temperature (T_5), and $T_{c,out}$ is the exit cold fresh water temperature (T_6).

The main purpose of this analysis is to explore the performance boundaries of the DDD process. Specification of the system operating variables, however, is not arbitrary. Namely, there is a constraint that must be satisfied: the cold fresh water temperature leaving the condenser cannot be higher than the air inlet temperature. This is so the air

36

can always release heat to the cold fresh water during the dehumidification process. It is assumed $T_{c,out} = T_6 = T_{a,in}$.

Assuming the heat and mass transfer process in the condenser is similar to that of the diffusion tower, they will require the same height. The required pumping power for the condenser is evaluated as,

$$\frac{P_{DC}}{P_{Dif}} = \frac{m_c}{m_b} \qquad (39)$$

where P_{DC} and P_{Dif} are the required pump energy for the condenser and the diffusion tower respectively. This is obviously a gross assumption.

As an example, consider a 100 MW power plant where the thermal efficiency is 40%. The total input energy is then 250 MW and the waste heat is 150 MW. If the power plant is operating with 3" Hg pressure in the main condenser, there would be approximately 140 MW of energy at 46° C available from low pressure condensing steam. If retrofitted with a diffusion driven desalination (DDD) plant, there is a potential to produce as much as 1.03 million gallons/day of fresh water assuming the feed water temperature enters the diffusion tower at 46° C. The energy consumption from the seawater, air, and cold fresh water pumps in the DDD process is about 0.0053 kW-hr per kilogram of fresh water. Thus the electrical power requirement is 0.87 MW in total. And the total construction area is 1211 m^2. The thermal energy consumed in the humidification-dehumidification process is waste heat, and is not of concern for the economic analysis.

5.2 Fresh Water Production Cost For the DDD system

The fresh water production cost strongly depends on the process capacity, site characteristics and design features. The system capacity specifies the sizes for various process equipment, pumping units, and required heat exchanger surface areas. Site characteristics have a strong influence on the type of pretreatment and post-treatment equipment, and consumption rates of chemicals. Process design features affect consumption of electric power, heating steam and chemicals (Wangnick et al [20] and Hisham et al [21]). Production cost is divided into direct and indirect capital costs and annual operating costs. Direct capital costs include the purchase cost of major equipment, auxiliary equipment, land and construction. Indirect capital costs include labor, maintenance, and amortization. They are usually expressed as percentages of the total direct capital cost.

Land

The cost of land may vary considerably, from zero to a sum that depends on site characteristics. Government-owned plants normally have zero charges. Plants constructed under build-own-operate-transfer (BOOT) contracts with governments or municipalities can have near zero or greatly reduced charges. The price of the land near the coast area of Florida varies significantly from $1,000- 1,000,000 per acre.

Building construction

Construction costs vary from $100-1,000/m^2. This cost is site-specific and depends on the building type. Buildings could include a control room, laboratory, offices and workshops.

Process equipment

This category includes processing equipment, as well as instrumentation and controls, pipes and valves, electric wiring, pumps, process cleaning systems, and pre- and post-treatment equipment. These are some of the most expensive items, and their cost depends on the type of process and capacity. Equipment costs may be less than $1,000 (*e.g.,* a laboratory-scale RO unit used to treat low-salinity water). On the other hand, the equipment cost for a 100,000 m^3/day RO system could approach $50 million. MSF and MEE equipment is generally more expensive than that of RO systems — current estimates for a plant capacity of 27,000 m^3/day are $40 million. However, most fossil power plants located in rural areas use seawater as their cooling medium. A small portion of the cooling water is used for the DDD system. Because the concentration rate of the DDD process is small, there is almost no need to do post-treatment on the drain of the DDD system. Nevertheless the feed seawater flow is supplied by the main pumps used in the power plant's cooling system. So the cost of the pre-treatment, post-treatment and main feed seawater pump will not be included in the DDD system. The other process equipment costs vary according to different manufacturers from $45,000-$140,000.

Auxiliary equipment

The following are considered auxiliary equipment: open intakes or wells, transmission piping, storage tanks, generators and transformers, pumps, pipes and valves. The current analysis will not include these items.

As an example, consider the DDD system coupled with a 100 MW power plant. The capital cost calculations are based on the following assumptions:
1) interest rate $i = 5\%$
2) plant life $n = 30$ yr

3) amortization factor $ai = \dfrac{i(1+i)^n}{(1+i)^n - 1} = 0.0651$ /yr

4) plant availability $f = 0.9$
5) specific chemicals cost $k = 0$ as the reason illustrated before for DDD system
6) specific electric cost c=0, because it will be considered separately in the electricity production of the power plant
7) specific heating steam cost s=0, because waste heat from the power plant is used
8) specific cost of operating labor $\gamma = \$0.025 - 0.05/m^3$. It is typically $0.1/m^3$ for the thermal processes and $0.05/m^3$ for RO. Because the DDD is a low temperature and pressure process, the labor cost is assumed lower than for RO process

Table 2 Summary of direct costs

Name	Land	Building construction	Major equipment
Cost ($)	300-299,245	121,138-1,211,380	45,000-140,000
Total Direct Cost DC ($)	166,438-1,650,625		

Table 3 Details of direct costs calculations

Name	Formula	Result
Annual fixed charges A_{fixed} ($)	$A_{fixed} = ai \cdot DC$	10,835 - 107,456
Annual steam cost A_{steam} ($)	$A_{steam} = \dfrac{365 \cdot s \cdot \lambda \cdot f \cdot m_p}{PR \cdot 1000}$	0
Annual electric power cost A_{elec} ($)	$A_{elec} = c \cdot w \cdot f \cdot m_p \cdot 365$	0
Annual cost for chemicals A_{chem} ($)	$A_{chem} = k \cdot f \cdot m_p \cdot 365$	0
Annual labor cost A_{labor} ($)	$A_{labor} = \gamma \cdot f \cdot m_p \cdot 365$	31,975 – 63,959
Total annual cost A_{total} ($)	$A_{total} = A_{fixed} + A_{steam} + A_{elec} + A_{chem} + A_{labor}$	42,810 – 171,415
Unit product cost in terms of production $A_{unit,p}$ ($/m^3)	$A_{unit,p} = \dfrac{A_{total}}{f \cdot m_p \cdot 365}$	0.033 – 0.134
Unit product cost in terms of capacity $A_{unit,c}$ ($/m^3/day)	$A_{unit,c} = \dfrac{A_{total}}{m_p}$	10.99 – 44.02

The economic value of a 100 MW power plant (40% efficiency) with and without the DDD process is summarized in Table 4. The economic increase rate of the combined system is 2 - 3%.

Table 4 Comparison of the economic value of a power plant with and without DDD

Power Plant	Production		Cost ($)	Retail Price ($)	Profit ($/day)	Total Profit ($/day)	Economic Increase Rate
Without DDD	Electricity (MW)	100	0.05 /kWhr	0.073 /kWhr	55200	55200	0
With DDD	Electricity (MW)	99.13	0.05 /kWhr	0.073 /kWhr	54720	56361 - 56754	2.1 – 2.8%
	Fresh Water (million gal/day)	1.03	0.125-0.507 /10^{3}gal	2.1 /10^{3}gal	1641 - 2034		

Notes:
1. The cost and retail price of electricity is based on an investigation of Florida electricity utilities.
2. The profit = retail price – cost
3. The retail price of water is from a recent survey [24] by the NUS Consulting Group, based on the municipal water price as of July 1, 2002 in U.S.

An economic increase rate of the power plant combined with the DDD process for different fresh water prices is shown in Fig. 32. It is assumed to be a 100 MW power plant with 40% efficiency and the fresh water cost is $0.125 per 1000 gallon.
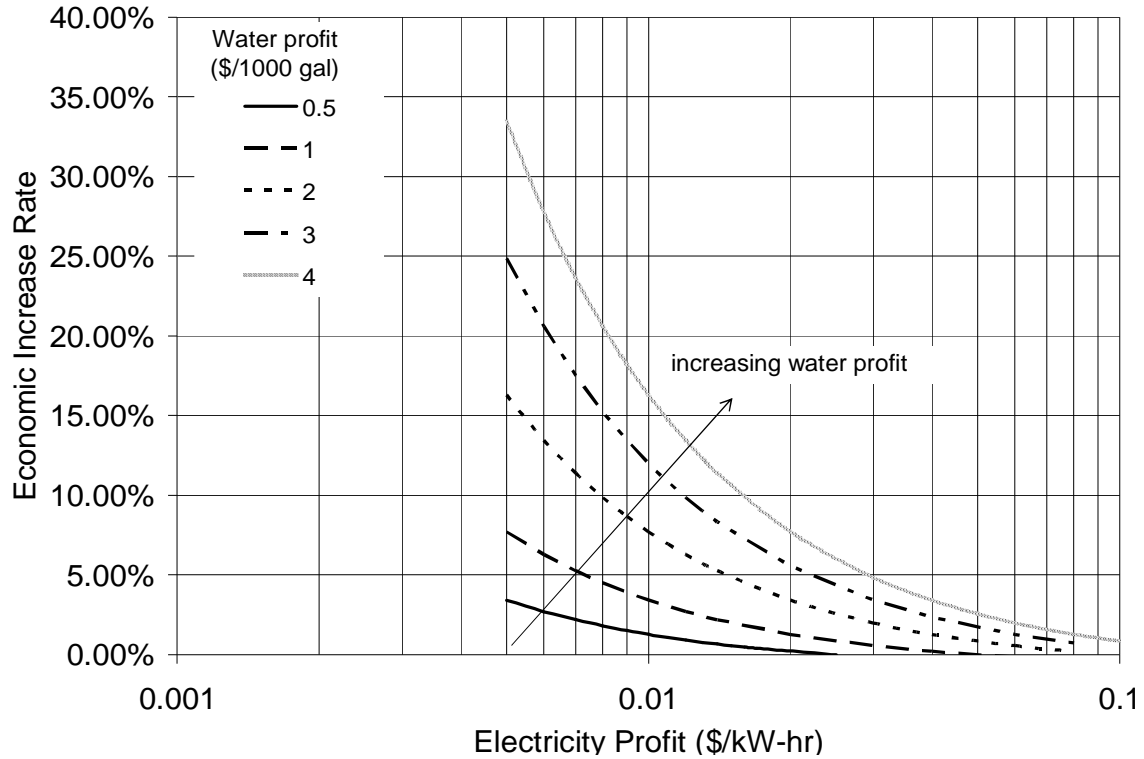
Figure 32 Economic increase rate with electricity profit for different fresh water profit

This figure clearly shows that the economic increase rate decreases with increasing electricity profit and the rate of decrease will slow down when the electricity profit is higher than $0.01/kW-hr. It is also important to note that the economic increase of the combined power plant tends to zero when the electricity profit is higher than $0.1/kW-hr, which is not likely for major fossil power plants.

From this figure, the economic increase rate is growing almost proportionally with the fresh water profit. It clearly shows that the combined power plant could have an economic increase when the fresh water is sold at a rate higher than $0.5/10^{3}gal. This price is strongly competitive with any other kind of seawater desalination system.

Finally, an investigation of the electricity market in the America is examined to explore the economic advantage of the DDD process within different geographical markets.

The average revenue in the United States for electricity generation [22] is $0.0693/kW-hr. The average electricity costs in Kentucky were $0.041/kW-hr during 2001, the lowest in the United States. The average revenue for all the states is shown in Fig. 33.
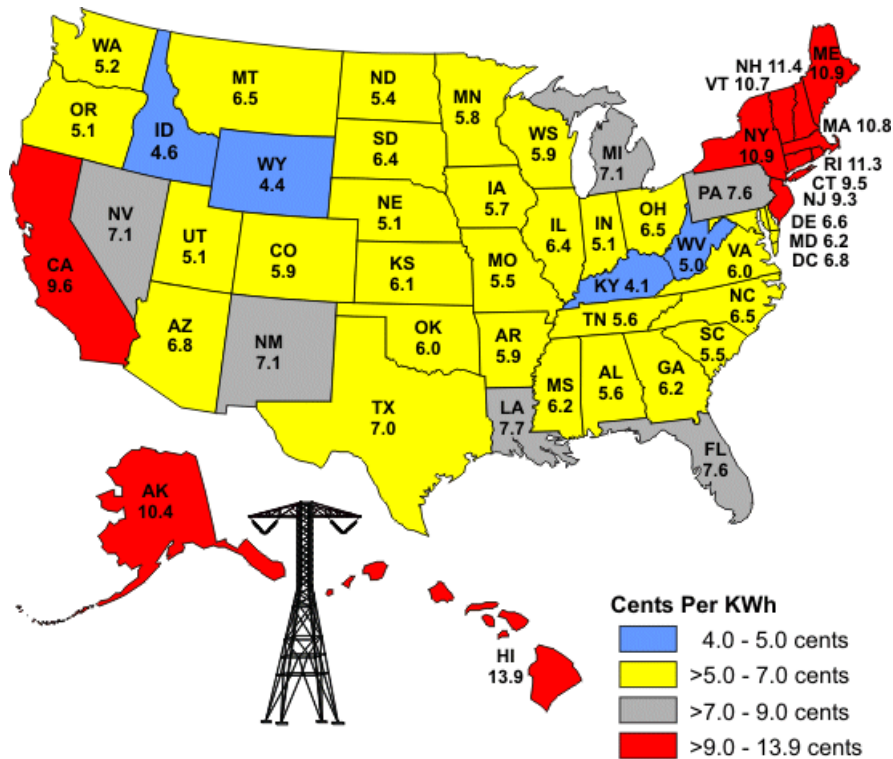
Figure 33 Average revenue ($/kW-hr) for all sectors of consumers by state, 2001

The cost of electricity (COE) is comprised of three components: capital and installation (C&I), operation and maintenance (O&M), and fuel (F). The total cost of electricity from an electric utility is the sum of these three components, expressed in dollars per kilowatt-hour: Total COE = C&I + O&M + F. The breakdown of the three components will vary with the size and type of equipment. However, California Energy Commission supplies a figure that provides an example of the breakdown for a 4.5 MW natural gas combustion turbine shown in Fig. 34.
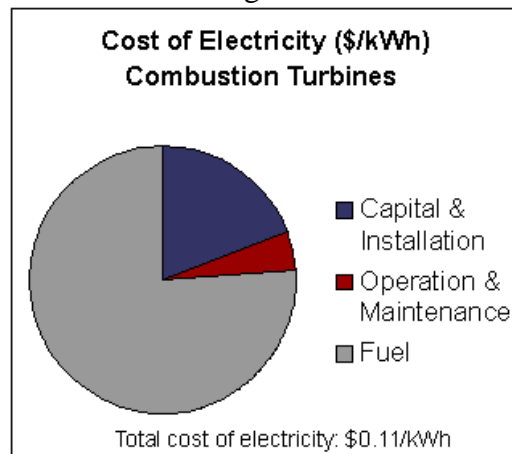
Figure 34 Electricity cost of a natural gas power plant in California

The total cost of electricity for this power plant is $0.11/kW-hr. Although the cost will come down by increasing the power plant capacity, the average cost in the whole country is still very high. This figure also clearly shows the fuel component is typically the largest portion of the cost of electricity in a system that utilizes fuel. It is unlikely that the price of fuel will come down in the future due to the limited supply of fossil fuel and increasing demand throughout the world.

Because of increasing concerns of environmental impact, the environmental costs of electricity are becoming more substantial. The U.S. Congress reports [23], the environmental cost for a coal power plant is $0.045/kW-hr, $0.047/kW-hr for an oil power plant, and $0.011/kW-hr for a natural gas power plant in the United States.

A recent survey [24] by the NUS Consulting Group studying water rates across the world found that rates increased in 12 of 14 countries surveyed. The result is shown in Table 5. The survey was based on prices as of July 1, 2002 for an organization with an annual usage of 10,000 cubic meters. Where there was more than a single supplier, an unweighted average of available prices was used. The percentage change for each country was calculated using the local currency in order to eliminate currency exchange distortion. Water rates in the United States were among the lowest in the countries surveyed and were one half to one third the rates charged in most European countries.

Table 5 Water price in different countries

	Ranking		Cost (US¢)	Change
	Current	Prior	Cubic meter	Year On Year
Germany	1	1	178.1	0.0%
Denmark	2	2	172.0	+0.8
United Kingdom	3	3	123.2	+3.2%
The Netherlands	4	4	113.8	-0.5
France	5	5	108.3	+3.3
Belgium	6	6	101.9	+3.9%
Italy	7	7	72.7	+1.5%
Spain	8	8	71.2	+3.5%
Finland	9	9	64.3	+4.9%
Sweden	10	10	61.5	+1.1%
Australia	11	11	54.7	+4.7%
United States	12	12	54.3	+4.0%
South Africa	13	14	42.8	+20.4%
Canada	14	13	37.6	+2.9%

Based on the above considerations, it is clear that there exists economic benefit for the DDD process to electric utilities. It is anticipated that this benefit will grow as the world fresh water supply continues to diminish.

6. Summary of Completed Tasks
The following project tasks have been completed:

1) Design and fabricate a lab scale diffusion tower and direct contact condenser
2) Assemble DDD facilities and instrument DDD facilities
3) Develop a numerical simulation tool for predicting heat, mass, and momentum transfer in the diffusion tower
4) Incorporate results from dynamic simulation into a thermodynamic heat and mass balance to predict overall system performance
5) Use numerical tools to investigate optimum design criteria and operating conditions in the diffusion tower
6) Conduct experiments on the diffusion tower to validate or calibrate computational model
7) Conduct experiments on the diffusion tower to calibrate the computational model of the air pressure drop through the packing material
8) Develop a computational model for predicting heat, mass, and momentum transfer in diffusion tower
9) Conduct DDD experiments to test condenser's effect on the fresh water production
10) Modify direct contact condenser and conduct experiments to observe the improvement of the fresh water production rate
11) Combine the dynamic model of the diffusion tower and thermodynamic model of the direct contact condenser to predict economic potential of the DDD system

7. Summary
The second year of work on the development of a Diffusion Driven Desalination facility has been completed, and the results are promising. A detailed analysis shows that the waste heat from a 100 MW power plant can be used to produce 1.03 million gallons of fresh water per day using the DDD process. The energy used to drive the process is low thermodynamic availability waste heat, and the only energy cost is that used to power the pumps and fans. An economic simulation of the DDD system shows that the production costs of the DDD combined power plant is very competitive compared with the costs required for reverse osmosis or flash evaporation technologies. A laboratory scale DDD facility, which includes the diffusion tower and direct contact condenser has been fabricated. The whole system has been fully instrumented for detailed heat and mass transfer measurements. Extensive measurements of the diffusion tower and direct contact condenser were made during this year to validate their simulated performance. The analytical model of the diffusion tower proves to be quite satisfactory in predicting the thermal performance of counter flow packed beds. Further work is required to analyze the packed bed direct contact condenser.

Although the Diffusion Driven Desalination facility is a promising technology for fresh water production using waste heat from electric power plants, current industry practice will limit its implementation until the value of fresh water sharply increases. The current practice of electric power plants is to pump a very large rate of cooling water through the main condenser so that the temperature rise of the water across the condenser is only about 6° C. The DDD requires the discharge water from the condenser to be approximately 40° C. This could be accomplished by lowering the flow rate through the

condenser and providing more heat transfer surface area to compensate for the reduced heat transfer rate. This would require a power plant installing a DDD facility to also replace or modify the main condenser. This is not a likely scenario. The best prospect for incorporating the DDD facility into an electric power plant for fresh water production is with the fabrication of new plants where the main condenser could be sized appropriately for the specified flow conditions.

References

[1]   Bourouni, K., M. Chaibi, M.T., and Tadrist, L., 2001, *Water desalination by humidification and dehumidification of air: State of the art*, Desalination, Vol. 137, Issues 1-3, pp. 167-176.

[2]   Al-Hallaj, S., Farid, M.M., and Tamimi, A.R., 1998, *Solar desalination with a humidification-dehumidification cycle: performance of the unit*, Desalination, Vol. 120, Issue 3, pp. 273-280.

[3]   Assouad, Y., and Lavan, Z., 1988, *Solar desalination with latent heat recovery*, Journal of Solar Energy Engineering, Vol. 110, Issue 1, pp. 14-16.

[4]   Muller-Holst, H., Engelhardt, M., Scholkopf, W., Jul 1999, *Small-scale thermal seawater desalination simulation and optimization of system design*, Desalination 122-3, 255-262.

[5]   Al-Hallaj, S., Selman, J.R., 2002, *A comprehensive study of solar desalination with a humidification – dehumidification cycle*, a report by the Middle East Desalination Research Center, Muscat, Sultanate of Oman.

[6]   Klausner, J.F., Li,Y., Mei, R., 2004, *Innovative diffusion driven desalination process*, Journal of Energy Resources Technology.

[7]   Larson, R.L., Albers, W., Beckman, J., and Freeman, S., 1989, *The carrier-gas process – a new desalination and concentration technology*, Desalination, Vol. 73, pp. 119-137.

[8]   Beckman, J.R., Sep 1999, *Innovative Atmospheric Pressure Desalination*, Desalination Research and Development Program Final report No. 52 for Department of Interior Agreement No. 98-FC-81-0049.

[9]   Beckman, J.R., Oct 2002, *Carrier-Gas Enhanced Atmospheric Pressure Desalination*, Desalination Research and Development Program Final report No. 92 for Department of Interior Agreement No. 99-FC-81-0186.

[10] Bharathan, D., Parsons, B.K., and Althof, J.A., 1988, *Direct-Contact Condensers for Open-Cycle OTEC Applications*, National Renewable Energy Laboratory Report SERI/TP-252-3108 for DOE Contract No. DE-AC02-83CH10093.

[11] Klausner, J.F., Mei, R., and Li,Y. et al., 2003, *Innovative Fresh Water Production Process for Fossil Fuel Plants*, U.S. DOE - Energy Information Administration annual report.

[12] F. Merkel, Verdunstungskuhlung, VDI Forschungsarbeiten, 275, Berlin, 1925.

[13] D.R. Baker, H.A. Shryock, A comprehensive approach to the analysis of cooling tower performance, Journal of Heat Transfer, (1961) 339-350.

[14] J.W. Sutherland, Analysis of mechanical-draught counterflow air/water cooling towers, Journal of Heat Transfer, vol. 105, (1983) 576-583.

[15] F. Osterle, On the analysis of counter-flow cooling towers, International Journal of Heat and Mass Transfer, vol. 34, No. 4/5, (1991) 1316-1318.

[16] H.T.A. El-Dessouky, A. Ai-Haddad, F. Ai-Juwayhel, A modified analysis of counter flow wet cooling towers, Journal of Heat Transfer, vol. 119, (1997) 617-626.

[17] W.H. McAdams, J.B. Pohlenz, and R.C. St. John, Transfer of heat and mass between air and water in a packed tower, Chemical Engineering Progress, 45, (1949) 241-252.

[18] C.C. Huang, and J.R. Fair, Direct-contact gas-liquid heat transfer in a packed column, Heat Transfer Engineering, 10, No. 2, (1989) 19-28.

[19] K. Onda, H. Takechi, and Y. Okumoto, Mass transfer coefficients between gas and liquid phases in packed columns, Journal of Chemical Engineering of Japan, 1, (1968) 56-62.

[20] Wangnick, K. (2002), *2002 IDA Worldwide Desalting Plants Inventory Report No. 17*, produced by Wangnick Consulting for IDA, Gnarrenburg, Germany.

[21] Hisham M. Ettouney and Hisham T. El-Dessouky, Kuwait Univ., Ron S. Faibish and Peter J. Gowin, IAEA, *Evaluating the Economics of Desalination*, Chemical Engineering Progress, Dec. 2002, pp 32-39.

[22] U.S. DOE - Energy Information Administration, *Electric Power Monthly Annual*, August, 2001, U.S.

[23] From the Congress of the U.S - Office of Technology Assessment, *Studies of the Environmental Costs of Electricity*, September, 1994, U.S.

[24] Survey by the NUS Consulting Group, based on the municipal water price as of July 1, 2002 in U.S.

Appendix A Onda Correlation

$$k_L = 0.0051 \, \mathrm{Re}_{Lw}^{\,2/3} \, Sc_L^{\,-0.5} (ad_p)^{0.4} \left[\frac{\mu_L g}{\rho_L} \right]^{1/3}$$

$$k_G = 5.23 \, \mathrm{Re}_{GA}^{\,0.7} \, Sc_G^{\,1/3} (ad_p)^{-2} aD_G$$

$$^{\#}a_w = a \left\{ 1 - \exp \left[-2.2 \left(\frac{\sigma_c}{\sigma_L} \right)^{3/4} \mathrm{Re}_{LA}^{\,1/2} \, Fr_L^{\,-0.05} We_L^{\,1/5} \right] \right\}$$

$$\mathrm{Re}_{LW} = \frac{L}{a_w \mu_L} \quad \mathrm{Re}_{GA} = \frac{G}{a \mu_G} \quad \mathrm{Re}_{LA} = \frac{L}{a \mu_L}$$

$$Sc_L = \frac{\mu_L}{\rho_L D_L} \quad Sc_G = \frac{\mu_G}{\rho_G D_G} \quad Fr_L = \frac{L^2 a}{\rho_L g}$$

$$We_L = \frac{L^2}{\rho_L \sigma_L a}$$

$^{\#}$This equation has been modified from the original Onda correlation.

Appendix B DDD experimental data (without packing material in the condenser)

Diffusion tower

Seawater flow rate (kg/s)	Air flow rate (kg/s)	Seawater inlet temperature (C)	Seawater exit temperature (C)	Air inlet temperature (C)	Air inlet humidity
0.062	0.040	60.0	37.7	26.9	0.010

Direct contact condenser co-current stage

Cold water flow rate (kg/s)	Air inlet temperature (C)	Air exit temperature (C)	Air inlet humidity	Air exit humidity	Fresh water production rate (kg/hr)
0.005	42.4	38.5	0.056	0.045	1.63
0.070	42.3	35.9	0.056	0.039	2.46
0.081	42.2	35.2	0.056	0.037	2.66
0.098	41.6	34.3	0.054	0.035	2.72
0.110	41.4	33.8	0.053	0.034	2.79
0.123	41.7	33.5	0.054	0.034	2.96
0.119	41.9	33.5	0.055	0.034	3.05
0.109	42.1	33.8	0.055	0.034	3.02
0.092	41.6	34.4	0.054	0.035	2.69
0.075	42.1	35.6	0.055	0.038	2.46
0.006	42.3	38.8	0.056	0.046	1.42

Direct contact condenser countercurrent stage

Cold water flow rate (kg/s)	Air inlet temperature (C)	Air exit temperature (C)	Air inlet humidity	Air exit humidity	Fresh water production rate (kg/hr)
0.001	38.5	38.8	0.045	0.046	0.00
0.063	36.0	34.1	0.039	0.035	0.59
0.075	35.2	32.9	0.037	0.032	0.68
0.089	34.3	31.6	0.035	0.030	0.74
0.101	33.8	30.9	0.034	0.029	0.79
0.115	33.5	30.4	0.034	0.028	0.80
0.111	33.5	30.6	0.034	0.028	0.78
0.100	33.8	31.0	0.034	0.029	0.76
0.084	34.4	31.9	0.035	0.031	0.70
0.067	35.6	33.5	0.038	0.034	0.64
0.001	38.8	39.0	0.046	0.046	0.00

Diffusion tower

Seawater flow rate (kg/s)	Air flow rate (kg/s)	Seawater inlet temperature (C)	Seawater exit temperature (C)	Air inlet temperature (C)	Air inlet humidity
0.047	0.040	60.7	39.1	26.9	0.010

Direct contact condenser co-current stage

Cold water flow rate (kg/s)	Air inlet temperature (C)	Air exit temperature (C)	Air inlet humidity	Air exit humidity	Fresh water production rate (kg/hr)
0.006	40.5	37.3	0.050	0.042	1.19
0.069	40.4	35.0	0.050	0.037	1.87
0.073	40.0	34.5	0.049	0.036	1.93
0.086	40.1	33.8	0.049	0.034	2.21
0.100	40.2	33.2	0.049	0.033	2.44
0.118	40.0	32.7	0.049	0.032	2.53
0.123	39.8	32.5	0.049	0.032	2.50
0.107	39.8	32.9	0.049	0.032	2.38
0.090	39.7	33.4	0.048	0.033	2.21
0.074	40.0	34.2	0.049	0.035	2.03
0.006	40.2	36.9	0.050	0.041	1.26

Direct contact condenser countercurrent stage

Cold water flow rate (kg/s)	Air inlet temperature (C)	Air exit temperature (C)	Air inlet humidity	Air exit humidity	Fresh water production rate (kg/hr)
0.001	37.3	37.6	0.045	0.046	0.00
0.061	35.0	33.4	0.039	0.035	0.52
0.066	34.5	32.8	0.037	0.032	0.50
0.079	33.8	31.8	0.035	0.030	0.59
0.092	33.2	30.9	0.034	0.029	0.64
0.110	32.7	30.2	0.034	0.028	0.65
0.113	32.5	30.0	0.034	0.028	0.65
0.097	32.9	30.5	0.034	0.029	0.62
0.080	33.4	31.4	0.035	0.031	0.55
0.066	34.2	32.6	0.038	0.034	0.48
0.001	36.9	37.0	0.046	0.046	0.00

Diffusion tower

Seawater flow rate (kg/s)	Air flow rate (kg/s)	Seawater inlet temperature (C)	Seawater exit temperature (C)	Air inlet temperature (C)	Air inlet humidity
0.065	0.041	51.4	36.4	26.8	0.010

Direct contact condenser co-current stage

Cold water flow rate (kg/s)	Air inlet temperature (C)	Air exit temperature (C)	Air inlet humidity	Air exit humidity	Fresh water production rate (kg/hr)
0.006	37.0	34.0	0.041	0.034	0.98
0.071	36.9	32.3	0.041	0.031	1.41
0.088	36.5	31.6	0.040	0.030	1.46
0.097	36.5	31.5	0.040	0.030	1.55
0.110	36.8	31.2	0.041	0.029	1.67
0.123	37.2	31.0	0.042	0.029	1.86
0.117	37.3	31.0	0.042	0.029	1.89
0.098	37.0	31.5	0.041	0.030	1.68
0.079	37.1	32.1	0.042	0.031	1.55
0.006	37.2	34.5	0.042	0.036	0.90

Direct contact condenser countercurrent stage

Cold water flow rate (kg/s)	Air inlet temperature (C)	Air exit temperature (C)	Air inlet humidity	Air exit humidity	Fresh water production rate (kg/hr)
0.001	34.0	34.2	0.034	0.035	0.00
0.062	32.3	31.3	0.031	0.029	0.33
0.079	31.6	30.2	0.030	0.027	0.40
0.088	31.5	30.0	0.030	0.027	0.42
0.100	31.2	29.5	0.029	0.026	0.45
0.116	31.0	29.2	0.029	0.026	0.45
0.108	31.0	29.3	0.029	0.026	0.45
0.089	31.5	29.9	0.030	0.027	0.44
0.071	32.1	30.8	0.031	0.029	0.35
0.001	34.5	34.7	0.036	0.036	0.00

Appendix C DDD experimental data (with packing material in the condenser)

Diffusion tower

Seawater flow rate (kg/s)	Air flow rate (kg/s)	Seawater inlet temperature (C)	Seawater exit temperature (C)	Air inlet temperature (C)	Air inlet humidity
0.078	0.039	61.3	39.3	27.8	0.011

Direct contact condenser co-current stage

Cold water flow rate (kg/s)	Air inlet temperature (C)	Air exit temperature (C)	Air inlet humidity	Air exit humidity	Fresh water production rate (kg/hr)
0.005	40.3	36.8	0.050	0.040	1.48
0.069	41.7	33.0	0.054	0.032	3.03
0.084	42.3	32.5	0.056	0.031	3.46
0.095	42.2	32.1	0.055	0.030	3.54
0.105	41.8	31.7	0.054	0.030	3.44
0.104	41.8	31.7	0.054	0.030	3.43
0.090	41.9	32.1	0.055	0.031	3.36
0.080	42.4	32.6	0.056	0.032	3.45
0.065	42.2	33.5	0.055	0.033	3.07

Direct contact condenser countercurrent stage

Cold water flow rate (kg/s)	Air inlet temperature (C)	Air exit temperature (C)	Air inlet humidity	Air exit humidity	Fresh water production rate (kg/hr)
0.001	36.8	36.1	0.040	0.039	0.23
0.061	33.0	28.7	0.032	0.025	0.98
0.078	32.5	27.9	0.031	0.024	1.04
0.088	32.1	27.5	0.030	0.023	1.04
0.098	31.7	27.3	0.030	0.023	0.98
0.097	31.7	27.3	0.030	0.023	0.97
0.083	32.1	27.3	0.031	0.023	1.07
0.073	32.6	27.6	0.032	0.023	1.15
0.059	33.5	28.4	0.033	0.025	1.19

Diffusion tower

Seawater flow rate (kg/s)	Air flow rate (kg/s)	Seawater inlet temperature (C)	Seawater exit temperature (C)	Air inlet temperature (C)	Air inlet humidity
0.057	0.041	59.1	37.6	28.2	0.011

Direct contact condenser co-current stage

Cold water flow rate (kg/s)	Air inlet temperature (C)	Air exit temperature (C)	Air inlet humidity	Air exit humidity	Fresh water production rate (kg/hr)
0.005	40.3	37.0	0.050	0.041	1.37
0.070	40.7	32.9	0.051	0.032	2.73
0.080	40.6	32.2	0.051	0.031	2.96
0.091	40.4	31.7	0.050	0.030	2.99
0.107	40.5	31.3	0.050	0.029	3.15
0.103	40.4	31.3	0.050	0.029	3.11
0.088	40.7	31.7	0.051	0.030	3.04
0.070	40.8	32.6	0.051	0.031	2.75

Direct contact condenser countercurrent stage

Cold water flow rate (kg/s)	Air inlet temperature (C)	Air exit temperature (C)	Air inlet humidity	Air exit humidity	Fresh water production rate (kg/hr)
-0.001	37.0	36.5	0.041	0.040	0.12
0.062	32.9	29.0	0.032	0.026	0.89
0.073	32.2	28.0	0.031	0.024	0.96
0.083	31.7	27.6	0.030	0.024	0.90
0.099	31.3	27.4	0.029	0.023	0.83
0.095	31.3	27.5	0.029	0.023	0.83
0.080	31.7	27.6	0.030	0.024	0.90
0.074	32.1	27.7	0.030	0.024	0.98
0.063	32.6	28.1	0.031	0.024	1.02

Nomenclature

A	control surface area (m^2)
a	specific area of packing material (m^2/m^3)
ai	amortization factor (yr^{-1})
C_{drag}	aerodynamic drag on droplet
C_p	specific heat of air (kJ/kg)
c	electric cost, ($\$/m^3$)
D	molecular diffusion coefficient (m^2/s)
DC	direct capital cost (\$)
dp	diameter of the packing material (m)
E	Power from a power plant (MW)
f	plant availability
G	air mass flux (kg/m^2-s)
g	gravitational acceleration (m/s^2)
H	diffusion tower height (m)
h	enthalpy (kJ/kg)
h_{fg}	latent heat of vaporization (kJ/kg)
i	interest rate
k	specific chemicals cost ($\$/m^3$)
k_G	mass transfer coefficient (m/s)
L	water mass flux (kg/m^2-s)
M_V	vapor molecular weight (kg/kmol)
m	mass flow rate (kg/s)
m_{drop}	mass of an individual droplet (kg)
m_p	plant capacity (m^3 /day)
n	plant life (yr)
P_a	partial pressure of air (Pa or kPa)
P_{sat}	partial pressure of vapor (Pa or kPa)
P	electrical power consumption for pumps (W, kW or MW)
PR	performance ratio (kg product/kg steam)
q	heat exchanged in condenser (W)
R	universal gas constant (kJ/kmol-K)
R_a	engineering gas constant for air (kJ/kg-K)
r	energy convert efficiency
S	heating steam cost (\$/MkJ)
T	temperature (°C or °K)
U	heat transfer coefficient (W/m^2-K)
u	air/vapor velocity (m/s)
V	control volume (m^3)
V_G	air/vapor volume flow rate (m^3/s)
v_d	droplet velocity (m/s)
w	specific consumption of electric power (kWh/m^3)
Φ	relative humidity
ω	humidity ratio

μ	dynamic viscosity (kg/m-s)
ρ	density (kg/m^3)
σ_L	surface tension of liquid (N/m)
σ_C	critical surface tension of the packing material (N/m)
γ	specific cost of operating labor ($/m^3)
γ_d	mass transfer coefficient for droplet condensation (m/s)
λ	average latent heat of steam (kJ/kg)

Subscripts

a	air
b	seawater
c	cold fresh water
DC	direct contact condenser
Dif	diffusion tower
DDD	DDD system
d	droplet
elec	electricity
evap	the portion of liquid evaporated
fw	fresh water
H	high
i	interface
L	low
l	water in liquid phase
mix	air/vapor mixture
nopack	without packing
v	water in vapor phase
in	inlet parameter
out	exit parameter
pack	with packing
s	steam
sat	saturate state
Total	total input
waste	waste